NUMERICAL STUDY ON SHIP MOTION WITH LNG TANK SLOSHING

NURJANNAH BINTI HASBULLAH

UNIVERSITI TEKNIKAL MALAYSIA MELAKA

NUMERICAL STUDY ON SHIP MOTION WITH LNG TANK SLOSHING

NURJANNAH BINTI HASBULLAH

This report is submitted
in fulfillment of the requirement for the degree of
Bachelor of Mechanical Engineering

Faculty of Mechanical Engineering

UNIVERSITI TEKNIKAL MALAYSIA MELAKA

2020

DECLARATION

I declare that this project report entitled "Numerical Study on Ship Motion with LNG Tank Sloshing" is the result of my own work except as cited in the references

Signature : ....

Name : ....

Date : ....

APPROVAL

I hereby declare that I have read this project report and in my opinion this report is sufficient in terms of scope and quality for the award of the degree of Bachelor of Mechanical Engineering.

Signature	:.	....
Supervisor's Name	:	....
Date	:	....

DEDICATION

To my supervisor Dr. Mohamad Shukri bin Zakaria, PhD,

My late father Hasbullah bin Ramli,

My lovely mother Masitah binti Hanapiah,

My fellow friends,

Brother and Sisters,

Thank you for everything.

ABSTRACT

Ship motions excites the LNG tank sloshing in ship cargo when there is a violent sea waves, which causes impact load on tank wall and then influences the ship movement. Focusing on the Open Field Operation and Manipulation (OpenFOAM) development platform of the open source Computational Fluid Dynamics (CFD), numerical calculation of ship motion with tank sloshing is attained and the correlating numerical simulation and verification is performed. For this process, the waves and tank sloshing interactions are fully taken into account. The liquid sloshing motion in membrane tank is firstly simulate through six degrees of freedom motion. Liquid filling levels are set as 25%, 50%, 75% and 90% of the tank's volume, respectively, in order to find the highest maximum pressure. Then, the simulation is further conducted using baffles in order to control the maximum impact pressure in membrane tank. The key findings are: the impact pressure for 75% filling level of LNG is highest comparing to the other filling levels. The maximum impact of pressure for combinatorial baffles greatly reduced by 28% comparing with the tank with no baffle case.

ABSTRAK

Gerakan kapal menggerakkan tangki kargo kapal disebabkan oleh ombak kuat, yang menyebabkan beban hentakan pada dinding tangki dan kemudian mempengaruhi pergerakan kapal. Berfokus pada platform pengembangan Operasi dan Manipulasi Lapangan Terbang (OpenFOAM) dari sumber terbuka Dinamika Fluid Dinamik (CFD), pengiraan berangka pergerakan kapal dengan tangki pemendapan dicapai bersama simulasi dan verifikasi berangka yang berkaitan dilakukan. Untuk proses ini, interaksi pengurangan gelombang dan tangki diambil kira sepenuhnya. Gerakan cecair pada tangki membran pertama disimulasikan melalui gerakan darjah kebebasan enam darjah. Tahap pengisian cecair ditetapkan masing-masing 25%, 50%, 75% dan 90% dari isipadu tangki, untuk mencari kes tekanan paling tinggi. Kemudian, simulasi dilanjutkan dengan mensimulasikan dengan menggunakan pengkadang untuk mengawal tekanan hentaman maksimum pada tangki membran. Penemuan utama adalah: tekanan impak untuk tahap pengisian LNG sebanyak 75% adalah paling tinggi berbanding dengan tahap pengisian yang lain. Kesan tekanan maksimum untuk baffle kombinasi berkurang sebanyak 28% berbanding dengan kes tangki tanpa penghadang.

ACKNOWLEDGEMENT

First and foremost, all praises and thanks to the God, the Almighty, for His showers of blessings throughout my research work to complete the thesis successfully. I would like to express my sincere gratitude to my research supervisor, Dr. Mohamad Shukri bin Zakaria for giving me the opportunity to do research and providing invaluable guidance throughout this research. His vision and motivation have deeply inspired me. It was a great privilege and honor to work and study under his guidance.

I am extremely grateful to my lovely mom, Masitah binti Hanapiah for her love, prayers and sacrifices for educating and preparing me for my future. Also, I am very much thankful to my family for their loves, understanding, prayers and continuing support to complete this research work.

I would like to say thanks to my friends and colleagues especially Syahir Farhan bin Shamsuddin and Adibah Aqilah binti Shamsudin for their constant encouragement and their genuine support throughout this research work. Finally, my thanks go to all the people who have supported me to complete the research's work directly or indirectly

TABLE OF CONTENTS

LIST OF TABLES

LIST OF FIGURES

LIST OF ABBREVIATIONS

LNG	-	Liquefied Natural Gas
CFD	-	Computational Fluid Dynamics
2D	-	2 Dimensional
3D	-	3 Dimensional
VOF	-	Volume of Fluid
FDA	-	Food and Drug Administration

LIST OF SYMBOLS

ω	-	Angular frequency
f	-	Frequency
μ	-	Kinematic viscosity
ρ	-	Density
σ	-	Surface tension coefficient
κ	-	Curvature of surface interface
X_g	-	Displacement of mesh nodes
γ	-	Diffusivity
r	-	Distance between cell to the moving boundary
u	-	Velocity
p	-	Pressure
g	-	Gravity
Fs	-	Surface tension force
A	-	Amplitude

CHAPTER 1

INTRODUCTION

1.1 Background

LNG is the acronym for liquefied natural gas that has been made over millions of years of transformation of organic materials, such as plankton and algae. LNG is natural gas that has been cooled down to liquid form for safety and ease of non-pressurized storage. It is odorless, colorless, non-toxic and non-corrosive. LNG is normally stored in insulated tank at atmospheric pressure and typically boil slowly about giving off 0.10% - 0.15% of volume per day.

The beginnings of LNG's water bones started in 1950, Union Stockyards, Chicago and Continental Oil explored an early concept for the transportation and the uses of LNG. They planned to buy the gas in Gulf Coast, then liquefy it. After that, transport the oil to Chicago by the water and vaporize it for refrigeration by the cold in food processing industry and also make the gas available for using in the industrial field.

The *Methane* was built in Ingalls Shipyard with a capacity of cargo of 5,550 cubic meters and the purpose is to run on the Mississippi transportation of LNG north to Chicago. That current initial economics was looking good, but, due to the fear of contaminating the food product, Food and Drug Administration (FDA) was refused to give the permit to the concepts. The starting back of shipping the LNG happened when Continental choose to continue the operation of LNG and found the gas can be liquefied at Gulf coast, and then being transported to east Coast by water. After that, LNG was vaporized and they put into the main competitive and pipelining.

Figure 1.1 Methane’s LNG ship (Zalar et al., 2005)

LNG’s first regasification and production facilities in United States have been started operating in Cleveland, Ohio in year 1941. The facility is commonly called a top plant’s shaving. Since then, there are over hundred facilities in U.S which is situated near the centers of high request of natural gas.

Since the mid 1970’s, the size and the design of LNG carriers has remained relatively constant. The largest of these “conventional” carriers transport LNG cargoes ranging from 125000 m^3 to 145,000 m^3. Over this duration, the design and cost improvements were approximately incremental.

1.2 Problem Statement

Liquified Natural Gas (LNG) is transported by LNG ships and it will slosh in partially filled tanks. This will cause damage to tank structures. For examples, the tank structures will become cracks and fatigue, and it will affect the ship's stability.

Sloshing motion in a partially filled tank will be violent in certain condition. For instance, the frequency of the motion of the LNG tank is equal or closed to the natural frequency of the interaction between the LNG and the tank structure. So, there is a demand that the LNG carrier should be safely operated at all liquid filling level.

1.3 Objective

The objectives of this project are as follow:

a) To model sloshing phenomenon of LNG tank on the six degrees of freedoms motion responses using open source CFD software.

b) To investigate the effect of 25%, 50%, 75% and 90% filling capacity on pressure.

c) To analyze baffle design on reducing the pressure.

1.4 Scope of project

The scopes of present study are:

a) Sloshing motion analysis will be using numerical simulation only.

b) 3D geometry of sloshing tank.

c) Baffles design in the sloshing tank to reduce the sloshing load.

1.5 General methodology

The actions that need to be carried out to achieve the objectives in this project are listed below.

1. Literature review

   Select any related journals, articles or any other materials regarding this project and will be reviewed in the report.

2. Simulation

   Simulation of the Computational Fluid Dynamic (CFD) to get see the flow pattern in sloshing tank.

3. Analysis and proposed solution

   Analysis will be presented on how the sloshing tank level will affects the membrane tank. Solution will be presented based on the analysis of the baffles in the tank.

4. Report writing

   A report on this study will be written at the end of the project.

The methodology of this study is summarized in the flow chart as shown in Figure 1.2.

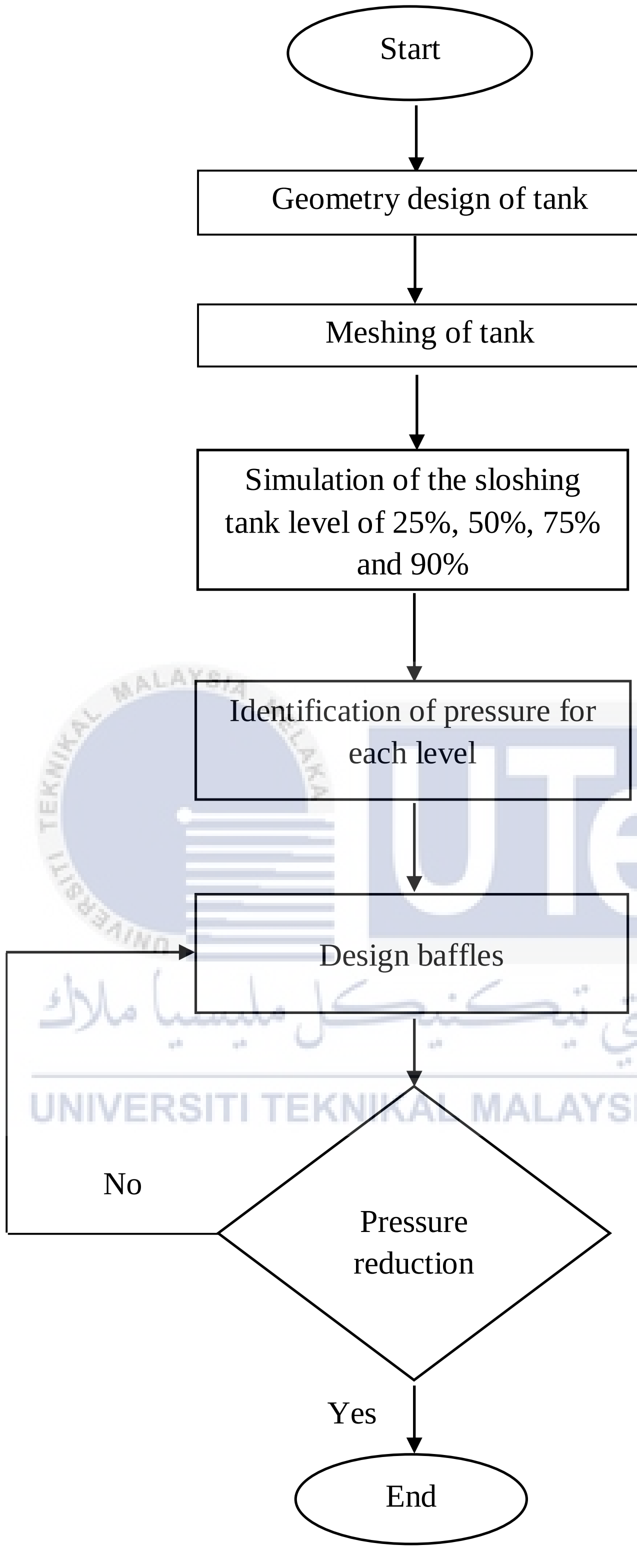

Figure 1.2 Flow chart of the methodology

CHAPTER 2

LITERATURE REVIEW

2.1 LNG carrier

As the liquefied natural gas (LNG) has increased in demand, LNG carrier continues and remain to experience astounding growth. The LNG shipper is a tank carrier invented for specific purpose which is transporting LNG and have commonly managed with fully tank loaded or a minimal loaded during the return voyages is at ballast. Figure 2.1 shows the LNG carrier's ship.

Figure 2.1 LNG Carrier's Ship (Zalar et al., 2005)

The common stuffing level of LNG tank is exceeding 95% tank height at the chock-full loaded condition and also below 5% at the condition of ballast (Kim et al., 2002). Afterwards the reconciliation of a broad chamfer on the top of tank. Then, augmented the insulation structure on the above part of tank that has been formed, the present design run-through which are underside scantling and padding system that has remained witnessed as a safe tank to a sloshing weight impact on some restricted operative circumstances (Tanaka et al., 1984). In the premature designs of LNG tank with a slighter smaller chamfer and decrepit padding scheme disclosed some amount of minimal compensations on padding part and the efficacy devices in tank as in Figure 2.2. Nonetheless, there is no indemnities have been informed in as much as the rise area of chamfer dimension and the strengthening of padding structure (Kim et al., 2002).

Figure 2.2 LNG Tank Shape (Kim et al., 2002)

2.2 Sloshing motion in LNG tank

Sloshing occurrence is a great conjectural and hands-on practical on importance in the littoral and offshore industrial with the considering to sea's safety on transporting the oils and LNG. Sloshing in a heavy sea waves may urge the physical damages toward the tank ramparts and also may distress the immovability of tank. Ship gestures are triggered by the convoluted contact between peripheral forces that wielded by the ocean waves on the underside of the body and also the forces exerted by the sloshing fluid inside the membrane ship tank (Peric, 2009).

Large deformation and impulsive pressure on the internal structure of tank happens because of the violent flow of the sloshing liquid in the tank. This happened when the external wave frequency is close to the motion of the ship with partially filled tanks. The excite motion of the ship will affect the loading impact since it is very sensitive to the motion.

There are some of the researchers done about the sloshing tanks just before the consideration on the effect of tank sloshing. Mikelis et al., (1984) have used a 2D finite element difference transient method to solve the pressure and the motion of liquid cargo. Other than that, Rognebakke and Faltinsen, (2000) were conducting a 2D experiments on the hull part that contain some tanks that filled with amount of water that excited by the waves. He also conducted the simulated model case by using the linear and non-linear sloshing model.

Kim et al. (2002) make a partition on the surface of tank by putting the number of panels as in Figure 2.3. The arrangement of every panels is determined from the typical arrangement of girders. Two of the numbers are defined at every panel. The maximum panel pressure is well-defined as the maximum value of the pressure's impact on the panel. Besides, immediate average impact pressure is the description of the average panel. It is a significant value for the input to the structural analysis since the bulkhead part is made with the even distribution load over the panel.

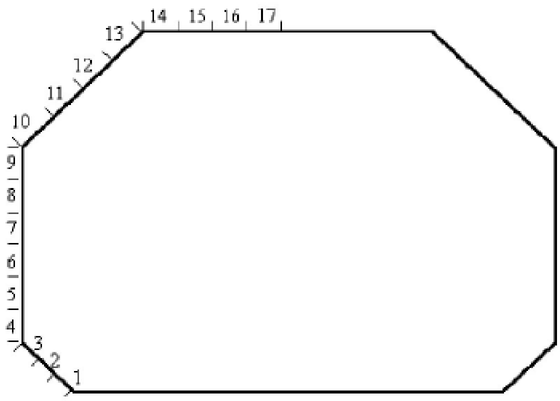

Figure 2.3 Panels used to determine the panel pressure (Kim et al., 2002)

2.3 Tank filling level

The sloshing gesture at the level of low filling is recognized to be absolutely dissimilar from the level of high filling. Standup waves were recognized in the tank at high level filling. When the filling level is lesser than 20% of the measurement of the tank, the dynamic waves are detected near the resonant conditions (Kim et al., 2002). The issue here is the strong point of the padding scheme to the influence weight. When at the half-done filling tank level, the widespread part on the fence of the tank is susceptible to the influence weight. The chamfer on upper of the knuckle points may experience a huge influence when the peak of standing surge at the container wall influences them.

Kim et al. (2002) observe that when the tank is in low filling level, the large impact of pressure occurred when the wave front of the hydraulic jumps hits and runs up the tank wall. A sharp peak of the pressure is formed due to large acceleration of the liquid run up at the wall. Figure 2.4 shows the results of the sloshing phenomena at the low filling level against time.

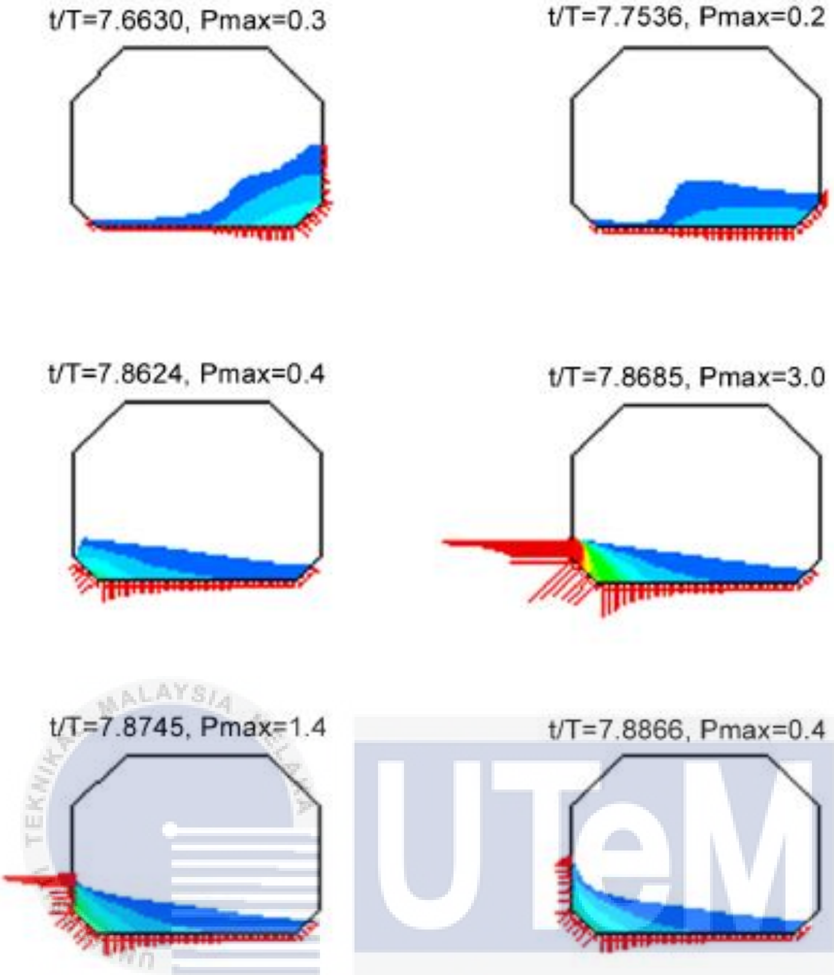

Figure 2.4 Distribution of pressure in the fluid domain and at the wall of the tank for low filling level (Kim et al., 2002)

Figure 2.5 shows the condition when the tank is in intermediate filling level, the free surface shape looks alike to the hydraulic jump at the low filling level . There is no pressure detected at the bulkhead part. The impact of pressure are experimental when the fluid reach the upper chamfer.

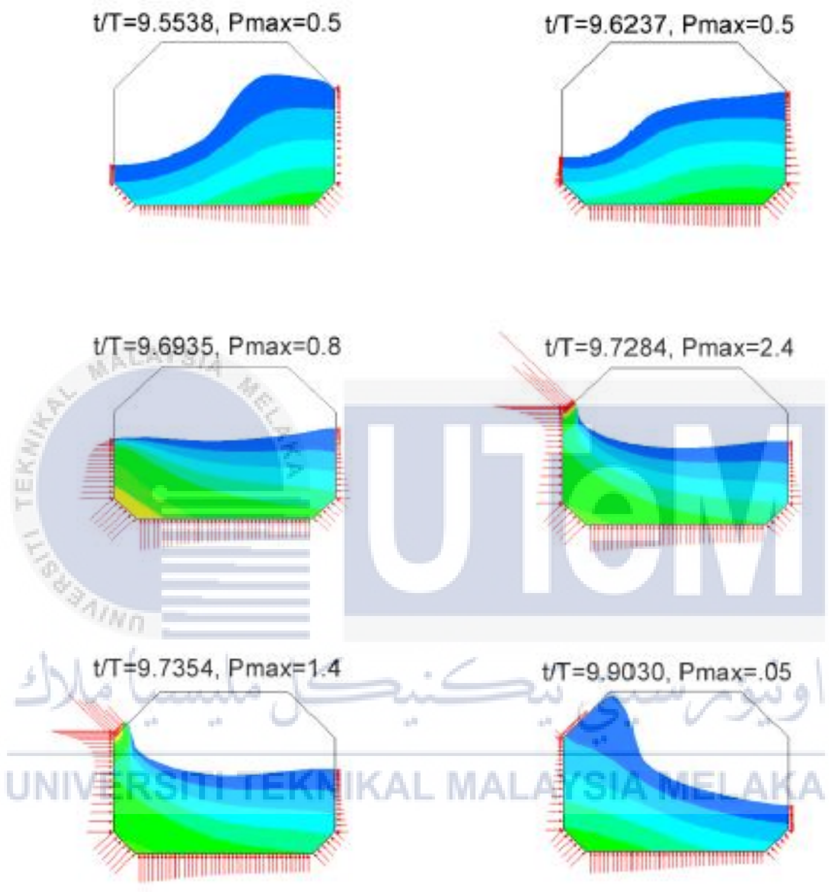

Figure 2.5 Distribution of pressure in the fluid domain and at the wall of the tank for intermediate filling level (Kim et al., 2002)

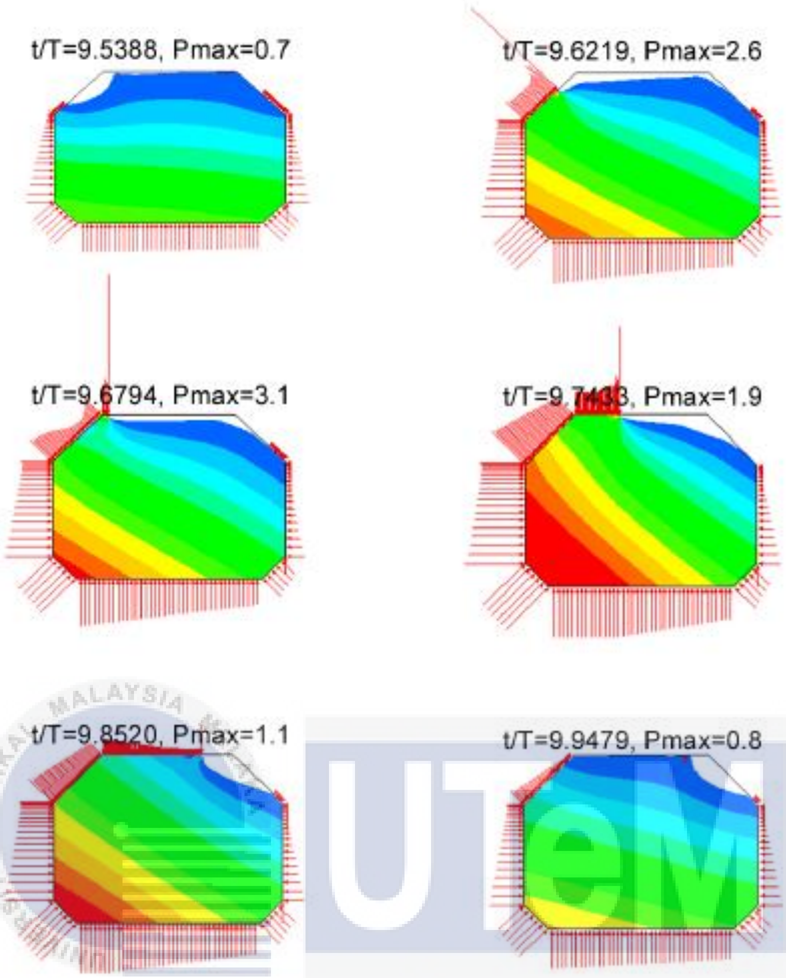

Figure 2.6 Distribution of pressure in the fluid domain and at the wall of the tank for high filling level (Kim et al., 2002)

In the Figure 2.6, the pressure has been detected at most of the surface of the tank. The liquid slosh in the tank hit the surfaces and this condition tend to make the surface become crack or broken since there are high pressure.

Time pressure history of the average and maximum panel pressure at three different filling level are shown in Figure 2.7. The result have been collected at T = 1.6s. As expected, the proportion of the average panel pressure to the maximum panel pressure at high filling level is smaller compare to the ratio at low filling level of the tank. The result where the pressure of impact at the bulkhead of the low filling level is the most significant compare to intermediate and high filling level. The reason why is this happening because the peak of impact load is highly localized at high filling level. This observation shows that the pressure's impact at high filling level has smaller effective area than the low filling level which is has wide effective area.

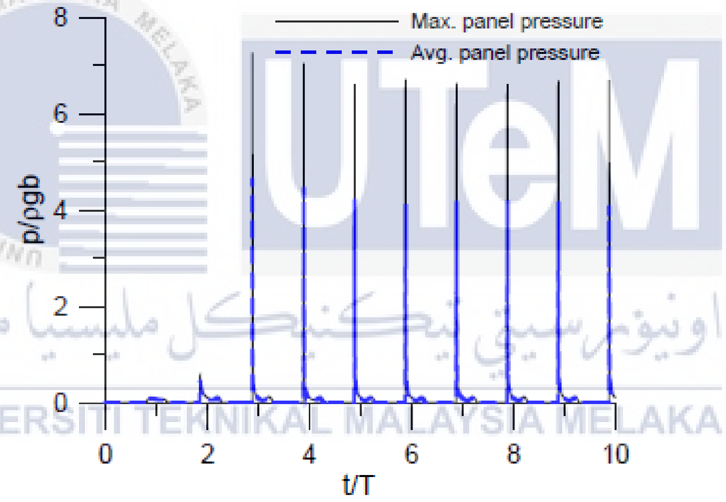

(a) Time pressure history at low filling level

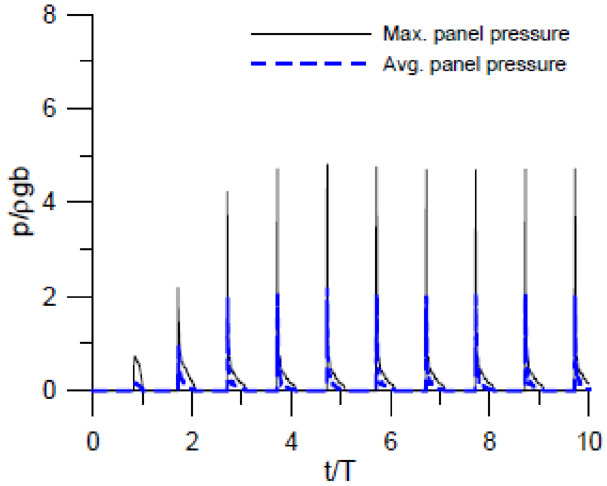

(b) Time pressure history at intermediate filling level

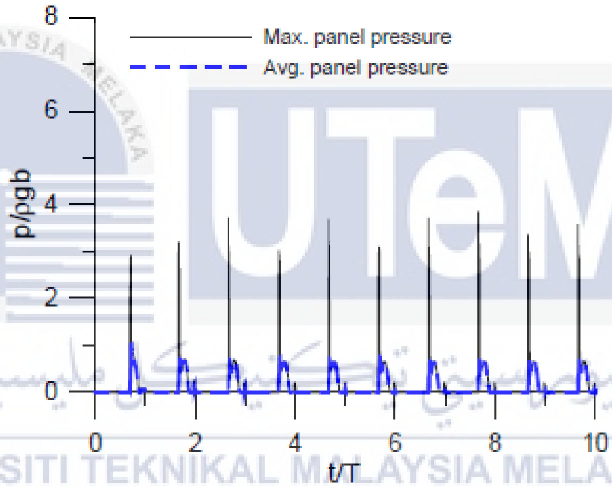

(c) Time pressure history at intermediate filling level

Figure 2.7 Time history of every filling level at T = 1.6 s (Kim et al., 2002)

2.4 Numerical Simulation

Hinatsu et al (2001) of the National Maritime Research Institute in Tokyo which is previously is Ship Research Institute, conducted an experiment a decade ago to evaluate the pressure on the tank walls on a different sloshing provisions. The consequences were broadly cast-off to validate simulation on numerical method. Although those experiment using the tank in a quadrangular shape, hence the outcomes cannot stay precisely transported to the common LNG containers. It is because of some walls of LNG tank is in inclined shape as in Figure 2.8.

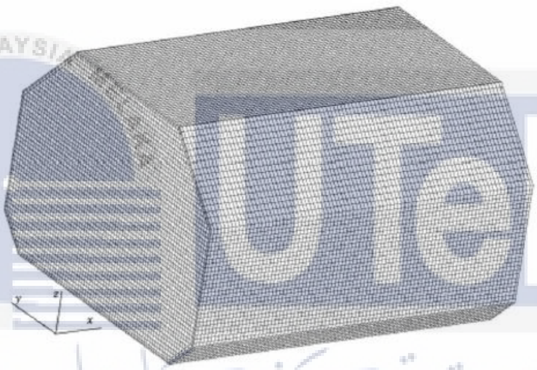

Figure 2.8 Geometry of the investigated tank (Peric et al., 2009)

2.4.1 Computational fluid dynamics (CFD)

The badly-behaved of sloshing fluid in the liquid tank is a typical problem in hydrodynamics in engineering circle. The research about fluid sloshing inside tank using CFD has become a big attention with the evolution of the specific fluid carriers, for instances which is Liquefied Petroleum Gas (LPG) and LNG. Thus, there are many investigators have carried a lot of investigates for this kind of circumstances. In the current study, viscous theory of flow is used to inspect on the performance of flow that happened in the tank sloshing. Besides, the theory is also have been used to investigate their persuaded influence weight over the simulating of the non-linear phenomenon (Yu-Long et al., 2011).

The evaluation of impact pressure in LNG tank using CFD numerical analysis is reliable. The pressure's impact is strictly contained in the time, and they are very sensitive to any effects such as gas entrapment, the type of surface's wall and even the small waves hit the surface. In such a complex condition, it might be difficult to use a manual experiment, so this phenomenon need to simulate by using numerical method where using much more computation step and refined mesh. However, when simulating using a long duration for LNG sloshing, CFD numerical simulations are actually restricted to a quite coarse model. The applicable information has been assembled by sloshing simulation of CFD that remains on the liquid's level kinematics, which is when the impact of sloshing is being computed by the velocity's impact with specific angle that related to the wall and also the geometry of LNG movement before the impact occurs.

With the growth of Computational Fluid Dynamics (CFD) approaches and computerisation methods, there are tons of numerical techniques have existed elaborate in the marketable software such as CFX, Fluent, Phoneics and any other more. Besides, the Open Field Operation and Manipulation (OpenFOAM) which is using of C++ programming languages. The archives have been supplied with dissimilar interlocks counting polyhedral mesh for conduct a multifaceted geometry in the recent years.

2.4.2 OpenFOAM

OpenFOAM is a free and a toolbox of open source CFD. It has been used in academic field and also used to solve a wide variation of computation problems that happened in the industry. There are numerous solvers and utilities provided by the OpenFOAM software which in a varied assortment of circumstances or problems that come out with a various meshes where including polyhedral mesh for a multifaceted geometry's handling. This software also provided with a pre-processing settings and the border to the pre-processing and post-processing are from OpenFOAM efficacies, by that safeguarding the reliable data conduct diagonally in all conditions.

With OpenFOAM, huge measure equivalent figuring also can be executed in this software. Furthermore, the handlers not using the OpenFOAM as a computing software, nonetheless also on using to adjust or change the encryptions in the software of OpenFOAM. Not only that, users can create an innovative solvers and numerical structures for appropriate glitches. Furthermore, the object-oriented of C++ programming linguistic puts a decent foundation for development of the OpenFOAM software, as glowing as the expansion of CFD (Yu-Long et al., 2011). The program of OpenFOAM can be refer to Appendix A-C.

2.5 Baffles in the Tank

A passionate sloshing can generate an extremely restricted influence potency on the tank divider or the ceiling area of the walls where might lead to injury or crack of the chamber. This impact force also may encourage necessary bulky moment to distress the constancy of the ship where the ship is carrying the tank with fluids, specifically when the peripheral excitation occurrence is adjacent to the significance occurrence (Xue et al., 2013). In command to diminish the possible of the slopping to make impairment, the controller of sloshing behaviour with there are baffles has existed a matter of attention in latest ages. But, the restraining appliance of the baffles is tranquil not a fully unspoken due to the difficulty and extremely non-linear countryside of the sloshing complications (Yan et al., 2001). Moreover, the lessons that have been carried and also the study on the sloshing subtleties are still exact noteworthy for LNG transporters or other runny liquid storage design container (Xue et al., 2013).

Additionally, those have become a huge cases of numerical research of fluid sloshing in LNG tank with number of baffles inside it during in the past of years. Kim (2001) did a simulation on sloshing movements in tanks with and also without the baffles by using a SOLA structure based on the resolving Navier-Stokes calculation and he establish that runny fluid is not forceful even they are in a great largeness excitation since the existence of baffles. Also, Kim and Lee (2008) concentrated on enhancing the measurement of length and the width of the baffles with purpose to diminish the effect of sloshing by smearing the evolutionary optimization method.

Figure 2.9 shows the 2D schematic diagram of LNG tank with a vertical baffle that insert in the middle of the tank where place it at the bottom of the tank.

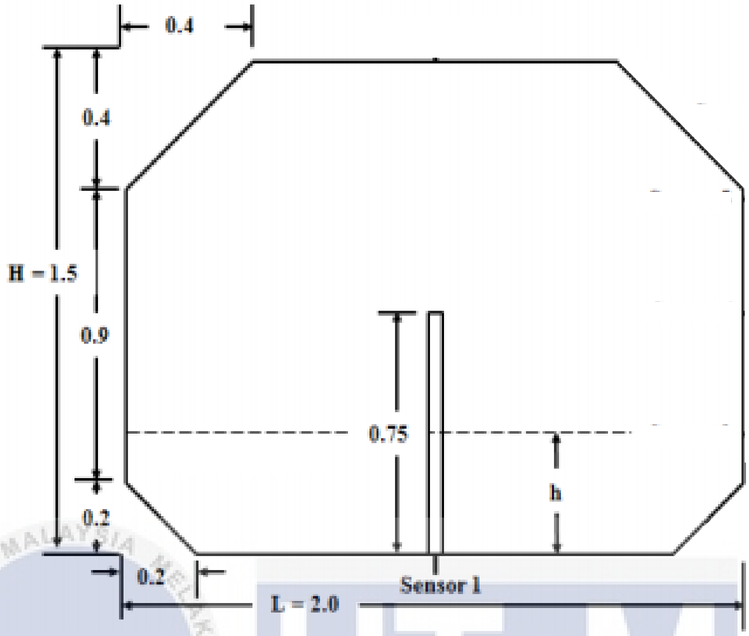

Figure 2.9 2D LNG tank with vertical baffle (Wei Wang et al., 2014)

CHAPTER 3

METHODOLOGY

3.1 Geometry of LNG Tank

The tank is in the form of a hexagon that has a length of 20 m on an x-direction. Then, it has a width of 40 m on the y-direction while 30 m is the depth of the tank on the z-direction. At the bottom of the tank, the depth to the top of lower chamfer is 5m and at the upper part, the height of upper chamfer is 10m. The angle of both lower and upper chamfer are 45° to the horizontal axis. The chamfer at the upper part is quite wide compare to the chamfer at the lower part due to the height of the chamfer is different. The dimension of LNG tank is listed in Table 3.1. The geometry and orthographic view of LNG tank are in Figure 3.1 and Figure 3.2 respectively.

Table 3.1 Dimension of LNG tank in full scale.

	Full scale
Length, x (m)	20
Breadth, y (m)	40
Height, z (m)	30

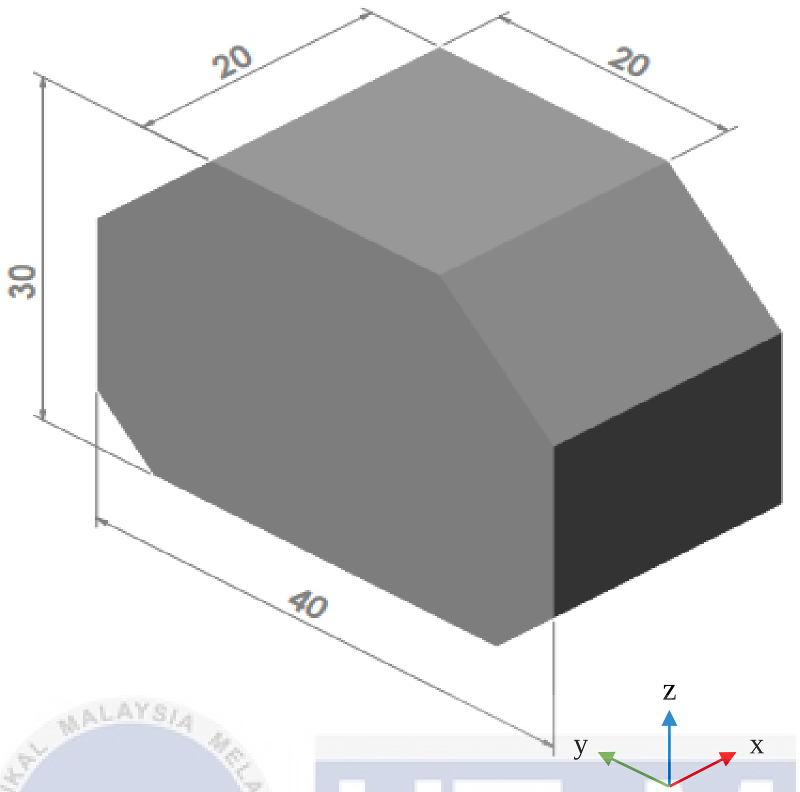

Figure 3.1 Geometry of LNG tank according to the dimensions

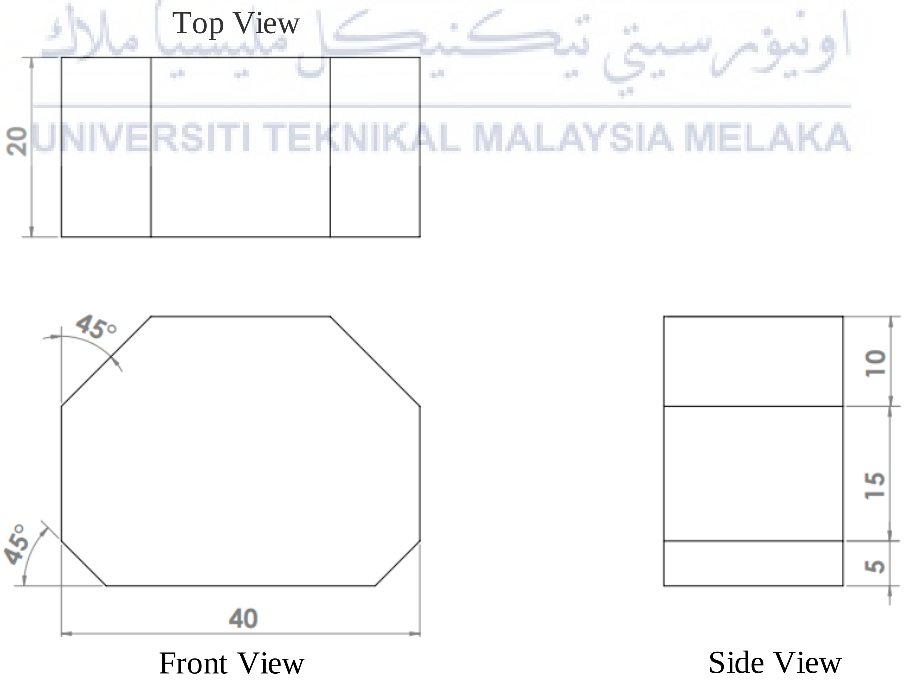

Figure 3.2 Orthographic view of LNG tank

3.2 Mesh of Tank

For number of cells in every part of the tank, there are 29 total of cells in the length while there are 50 cells in the breadth of the tank. The number of cells in the height of the lower chamfer has 16 cells and for the height of the upper chamfer has 22 cells. Besides, there are 26 number of cells in the height between the chamfers. Figure 3.3 shows the 3-dimensional of LNG tank with the number of cells.

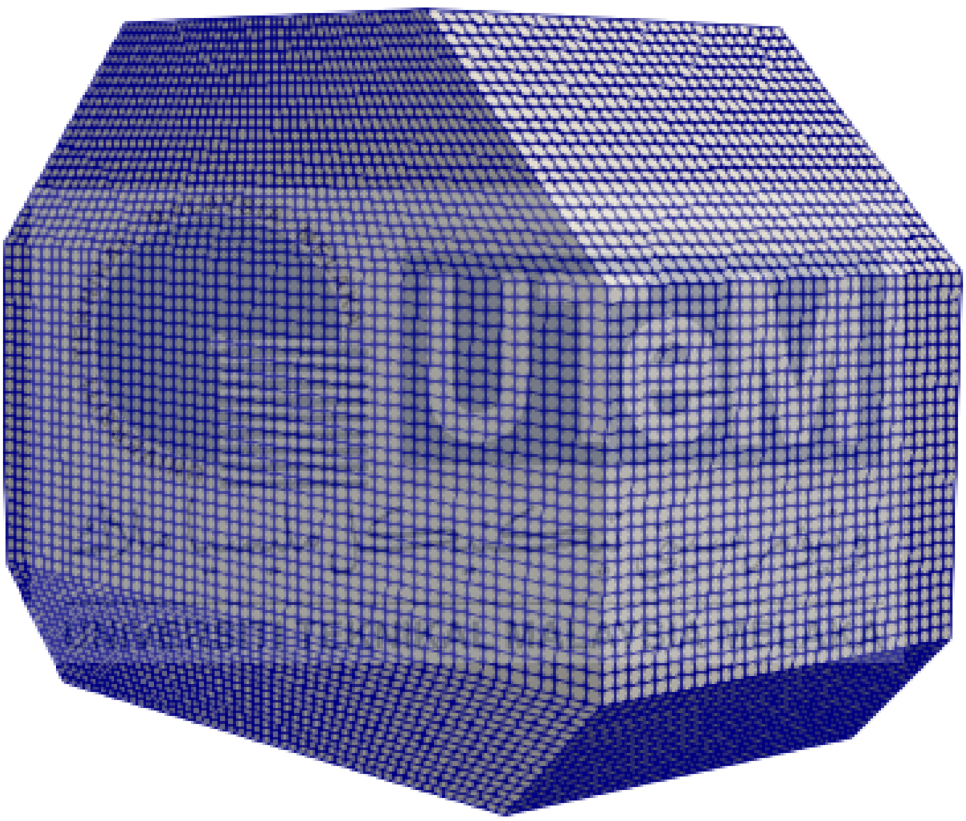

Figure 3.3 Mesh of LNG tank

3.3 Six-Degree of Freedom (6-DoF)

6-DoF module are fully implemented with the bodies. There are consists of two coordinates of the system. For translation, we described X, Y and Z while for rotation is X', Y' and Z'. Table 3.2 and 3.3 show the amplitude and frequency for translation and rotation respectively. The graph of translation movement of LNG tank has been shown in Figure 3.4, Figure 3.5 and Figure 3.6. For rotation movement, the graph has been shown in Figure 3.7, Figure 3.8 and Figure 3.9.

Table 3.2 Amplitude and frequency for translation

	X	Y	Z
Amplitude of translation, A (m)	2	3	2
Frequency of translation, *f* (rad/s)	0.5	0.8	0.4

Table 3.3 Amplitude and frequency for rotation

	X'	Y'	Z'
Amplitude of rotation, A (deg)	30	10	10
Frequency of rotation, *f* (rad/s)	0.4	0.7	0.5

The movement of translation of X is in harmonic motion as follows,

$$X = A \sin(\omega t) \tag{1}$$

where A denotes as an amplitude, t is time and ω is the angular frequency, determine by:

$$\omega = 2 \pi f \tag{2}$$

substitute value of *f* from Table 3.2 into eq. (2):

$$\omega = 2 \pi (0.5) \tag{3}$$

$$\omega = 3.142 \tag{4}$$

then, substitute value of A from Table 3.2 into eq. (1):

$$X = 2 \sin(3.142\, t) \tag{5}$$

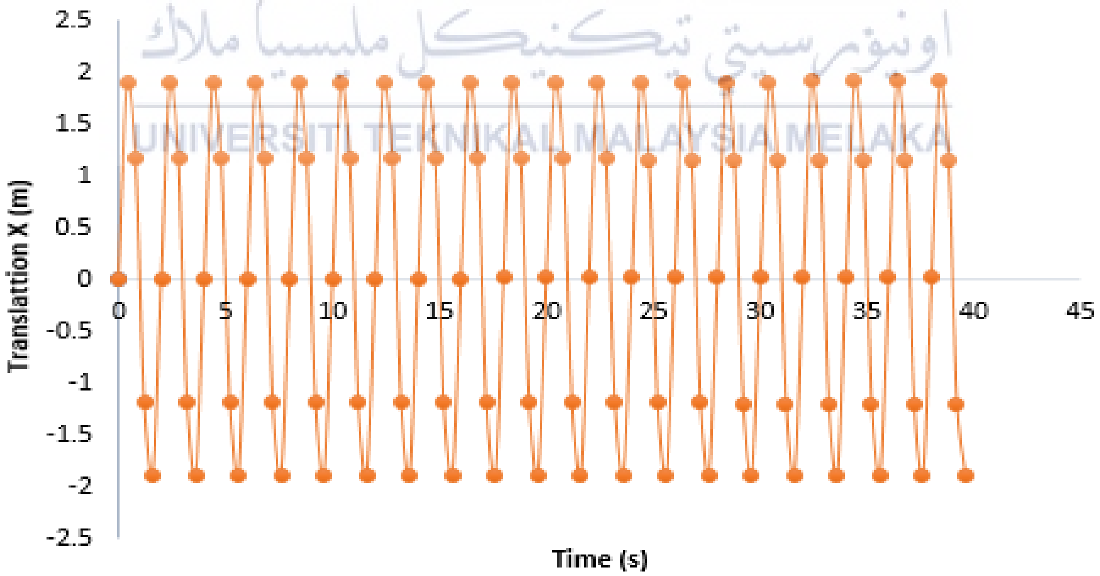

Figure 3.4 Translation graph in X-direction of LNG tank against time

The movement of translation of Y is in harmonic motion as follows,

$$Y = A \sin(\omega t) \tag{6}$$

where A denotes as an amplitude, t is time and ω is the angular frequency, determine by:

$$\omega = 2 \pi f \tag{7}$$

substitute value of *f* from Table 3.2 into eq. (7):

$$\omega = 2 \pi (0.8) \tag{8}$$

$$\omega = 5.027 \tag{9}$$

then, substitute value of A from Table 3.2 into eq. (6):

$$Y = 3 \sin(5.027 t) \tag{10}$$

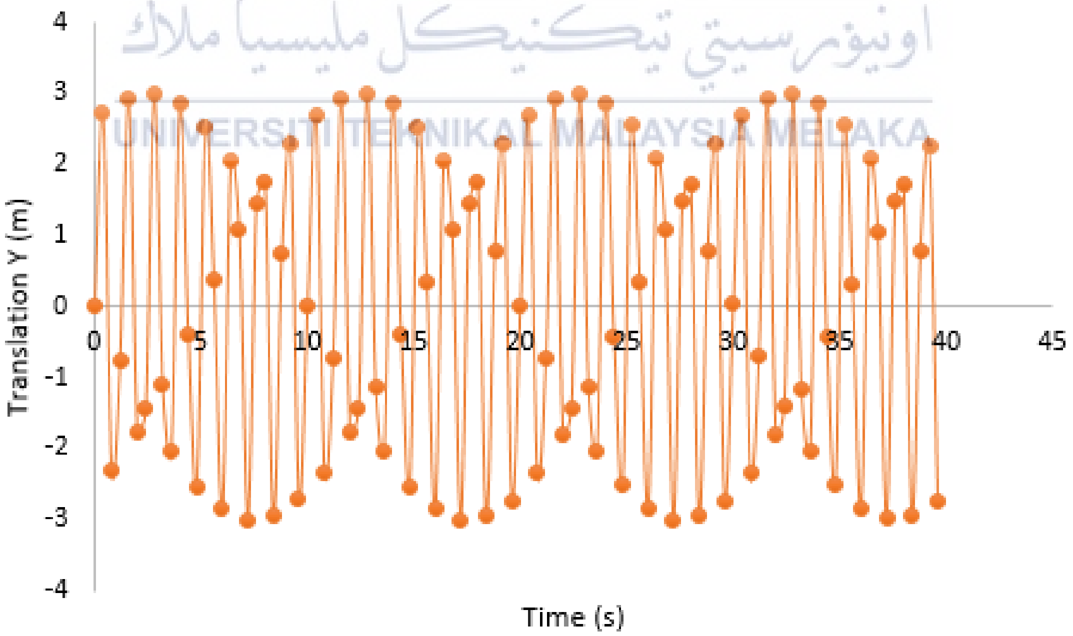

Figure 3.5 Translation graph in Y-direction of LNG tank against time

The movement of translation of Z is in harmonic motion as follows,

$$Z = A \sin(\omega t) \tag{11}$$

where A denotes as an amplitude, t is time and ω is the angular frequency, determine by:

$$\omega = 2 \pi f \tag{12}$$

substitute value of *f* from Table 3.2 into eq. (12):

$$\omega = 2 \pi (0.4) \tag{13}$$

$$\omega = 2.513 \tag{14}$$

then, substitute value of A from Table 3.2 into eq. (11):

$$Z = 2 \sin(2.513\, t) \tag{15}$$

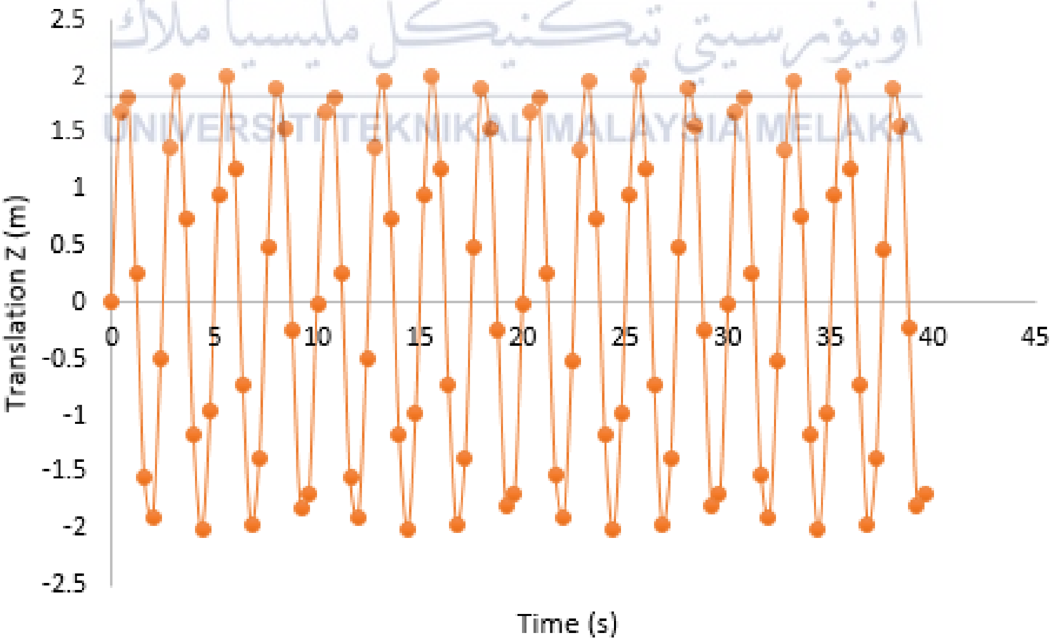

Figure 3.6 Translation graph in Z-direction of LNG tank against time

The movement of translation of X' is in harmonic motion as follows,

$$X' = A \sin (\omega t) \tag{16}$$

where A denotes as an amplitude, t is time and ω is the angular frequency, determine by:

$$\omega = 2 \pi f \tag{17}$$

substitute value of *f* from Table 3.3 into eq. (17):

$$\omega = 2 \pi (0.4) \tag{18}$$

$$\omega = 2.513 \tag{19}$$

then, substitute value of A from Table 3.3 into eq. (16):

$$X' = 30 \sin (2.513 t) \tag{20}$$

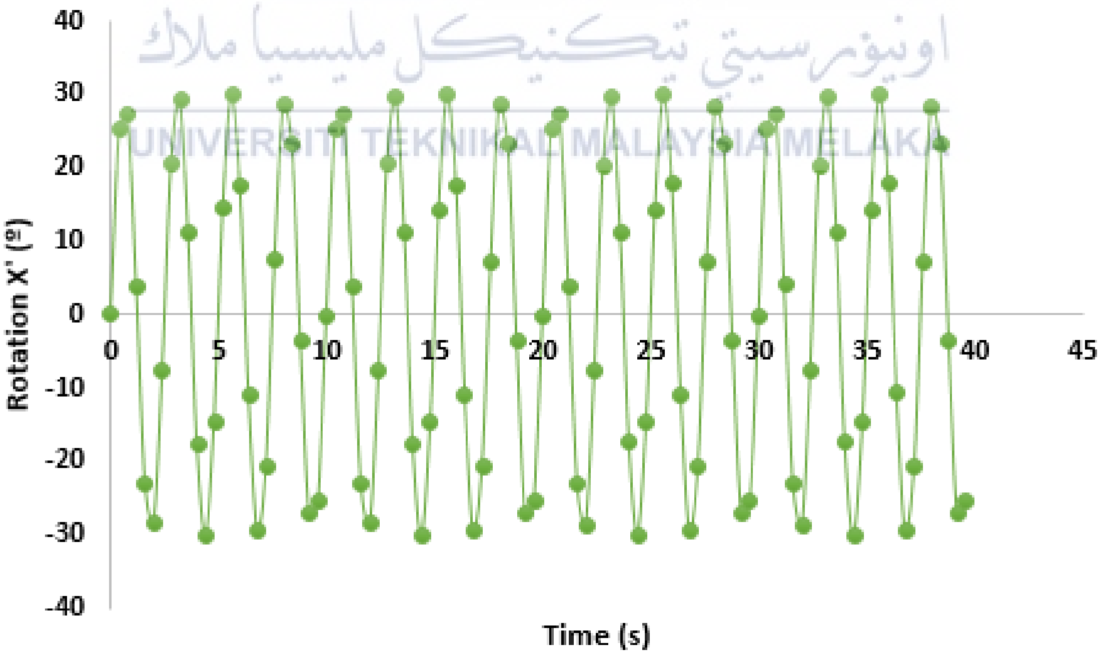

Figure 3.7 Rotation graph in X'-direction of LNG tank against time

The movement of translation of Y' is in harmonic motion as follows,

$$Y' = A \sin(\omega t) \tag{21}$$

where A denotes as an amplitude, t is time and ω is the angular frequency, determine by:

$$\omega = 2\pi f \tag{22}$$

substitute value of *f* from Table 3.3 into eq. (22):

$$\omega = 2\pi(0.7) \tag{23}$$

$$\omega = 4.398 \tag{24}$$

then, substitute value of A from Table 3.3 into eq. (21):

$$Y' = 10 \sin(4.398\, t) \tag{25}$$

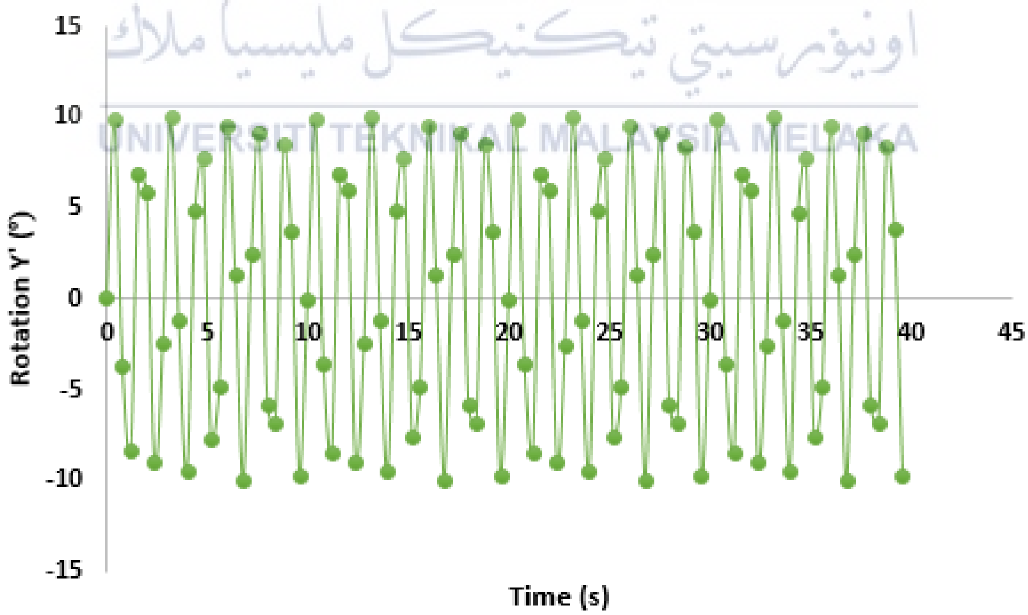

Figure 3.8 Rotation graph in Y'- direction of LNG tank against time

The movement of translation of Z’ is in harmonic motion as follows,

$$Z' = A \sin(\omega t) \tag{26}$$

where A denotes as an amplitude, t is time and ω is the angular frequency, determine by:

$$\omega = 2 \pi f \tag{27}$$

substitute value of *f* from Table 3.3 into eq. (27):

$$\omega = 2 \pi (0.5) \tag{28}$$

$$\omega = 3.142 \tag{29}$$

then, substitute value of A from Table 3.3 into eq. (26):

$$Z' = 10 \sin(3.142 t) \tag{30}$$

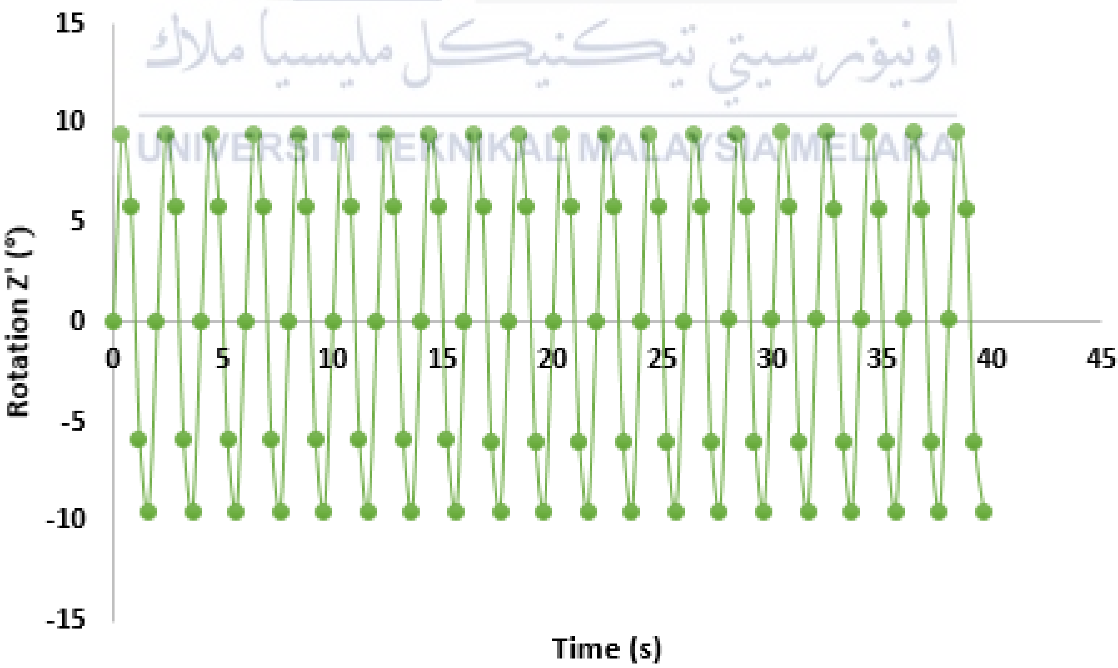

Figure 3.9 Rotation graph in Z’-direction of LNG tank against time

3.4 Dynamic Deforming Mesh

The ship motion and tank sloshing are solved as a whole, thus only the motion of ship needs the implementation of moving-mesh technique. In this paper, a kind of dynamic deforming mesh is used. The mesh deforms during the computation according to ship motion. The position of the mesh points in the field is solved by a Laplace equation with variable diffusivity:

$$\nabla \cdot (\gamma \nabla xg) = 0, \tag{31}$$

where x_g is displacement of mesh nodes; γ is diffusivity field, determined by

$$\gamma = 1/r^2, \tag{32}$$

where r is distance between cell centre to the moving boundary.

3.5 InterFOAM Solver

InterFOAM is one of the features of OpenFOAM code which is based on the finite volume method for two incompressible fluids. The interface is seized with a volume of fluid procedure. It is used to simulate the sloshing problematic.

The continuity equation is used to determine the conservation equation of mass. The equation for the continuity equation is reported as

$$\frac{\partial U}{\partial x} + \frac{\partial V}{\partial y} + \frac{\partial W}{\partial z} = 0. \tag{33}$$

In this study, the model uses a momentum equation with pressure-based solver. The momentum equation of the flow field is given by:

$$\frac{\partial u}{\partial t}+u\frac{\partial u}{\partial x}+v\frac{\partial u}{\partial y}+w\frac{\partial u}{\partial z}=-\frac{1}{\rho}\cdot\frac{\partial p}{\partial x}+f_x \tag{34}$$

$$\frac{\partial v}{\partial t}+u\frac{\partial v}{\partial x}+v\frac{\partial v}{\partial y}+w\frac{\partial v}{\partial z}=-\frac{1}{\rho}\cdot\frac{\partial p}{\partial y}+f_y \tag{35}$$

$$\frac{\partial w}{\partial t}+u\frac{\partial w}{\partial x}+v\frac{\partial w}{\partial y}+w\frac{\partial w}{\partial z}=-\frac{1}{\rho}\cdot\frac{\partial p}{\partial z}+f_z \tag{36}$$

The governing equations of incompressible fluid are as follow:

$$\begin{aligned}&\frac{\partial(\rho\vec{u})}{\partial t}+\nabla\cdot(\rho\vec{u}\cdot\vec{u})-\nabla\cdot\mu\nabla\vec{u}=\rho\vec{g}-\nabla p-\vec{F}_s\\&\nabla\cdot\vec{u}=0\end{aligned} \tag{37}$$

Where ρ denotes the density, u is the velocity vector, p is the pressure, μ is viscosity, g the gravity vector, and Fs is the surface tension force which only occurs at a free surface and not considered in sloshing simulation here.

In two phase problems, the physical properties of one fluid are calculated as the weighted averages based on volume fraction of water and air in one cell as follows,

$$\begin{aligned}\rho&=\alpha\rho_1+(1-\alpha)\rho_2\\\mu&=\alpha\mu_1+(1-\alpha)\mu_2\end{aligned} \tag{38}$$

Where $\rho 1$ and $\rho 2$ are the densities of the LNG and air, respectively, and is the volume fraction function for two fluids defined by:

$$\alpha=\begin{cases}1 & \text{volume occupied by LNG}\\0 & \text{volume occupied by air}\end{cases} \tag{39}$$

When $\alpha = 1$; $\rho = \rho 1$; $\mu = \mu 1$

When $\alpha = 0; \rho = \rho 2; \mu = \mu 2$

The volume fraction is transported by the velocity field and satisfies the following equation,

$$\frac{\partial \alpha}{\partial t} + \nabla \cdot (\alpha \vec{u}) = 0 \tag{40}$$

In OpenFOAM an extra artificial term is added to the VOF equation to obtain necessary surface compression as follows,

$$\frac{\partial \alpha}{\partial t} + \nabla \cdot (\alpha \vec{u}) + \nabla \cdot [\alpha(1-\alpha)\vec{u}_r] = 0 \tag{41}$$

Where u_f is the velocity field suitable to compress the interface. The artificial term is activated when the specified condition ($0 < \alpha < 1$) is satisfied.

3.6 Volume of Fluid (VOF)

The Volume of fluid (VOF) method with bounded compression techniques is applied to control numerical diffusion and capture the two-phase interface efficiently. The VOF transport equation is described below:

$$\partial\alpha / \partial t + \nabla \cdot [(U - Ug)\, \alpha] = 0, \tag{42}$$

where α is volume of fraction, indicating the relative proportion of fluid in each cell and its value is always between zero and one:

$$\begin{cases} \alpha = 0 & \text{air} \\ \alpha = 1 & \text{water} \\ 0 < \alpha < 1 & \text{interface.} \end{cases} \tag{43}$$

To capture the sharp interface and ensure conservation and boundedness, an extra term is added into VOF transport equation:

$$\partial\alpha/\partial t + \nabla \cdot [(U - Ug)\alpha] + \nabla \cdot [Ur(1 - \alpha)\alpha]=0. \quad (44)$$

The added term is nonzero only at interface, thus it doesn't affect solution at another region except interface. Ur in Eq. (44) is the velocity field used to compress the interface. It is normal to the interface so it does not affect the flow along interface. The description of Ur is given below:

$$\mathbf{U}_r = n_f \min\left\{c_\alpha \frac{|\varphi|}{|S_f|},\ \max\left(\frac{|\varphi|}{|S_f|}\right)\right\}, \quad (45)$$

where ϕ is face volume flux, S_f is normal vector of cell face. The recommended setting of $c\alpha$ is equal to 1, which maintains the sharp interface. Besides, the surface tension term is defined as:

$$f\sigma = \sigma\kappa\nabla\alpha, \quad (46)$$

where σ is the surface tension coefficient, which is chosen to be 0.07 kg/s2; κ is the curvature of surface interface, determined by volume of fraction α:

$$\kappa = -\nabla \cdot (\nabla\alpha/|\nabla\alpha|). \quad (47)$$

3.7 Model

In this study, the current flow is preserved as laminar and three-dimensional. For the fluid, which match up to LNG is supposed to be incompressible. The condition of the tank is in transient condition since the ship is moving against time.

3.8 Material Properties

There are two phases contained in the tank which are LNG and air. The material properties of each phase are shown in Table 3.4.

Table 3.4 Material properties of LNG and air

Properties	LNG	Air
Kinematic viscosity, μ	16.33×10^{-6} m^2/s	1.48×10^{-5} m^2/s
Density, ρ	468.1 kg/m^3	1 kg/m^3

3.9 Case Setup

To simulate the effect of pressure on the LNG tank, there are four types of filling level where the levels are 25%, 50%, 75% and 90% of LNG.

3.9.1 Liquid Filling Level

For this study, the liquid sloshing motion in membrane tank is firstly simulate through six degrees of freedom motion. Then, liquid filling levels are set to 25%, 50%, 75% and 90% of the tanks depth, respectively, in order to find the worst cases. 2-dimensional of LNG tank with different percentage of LNG filling level shown in Figure 3.10.

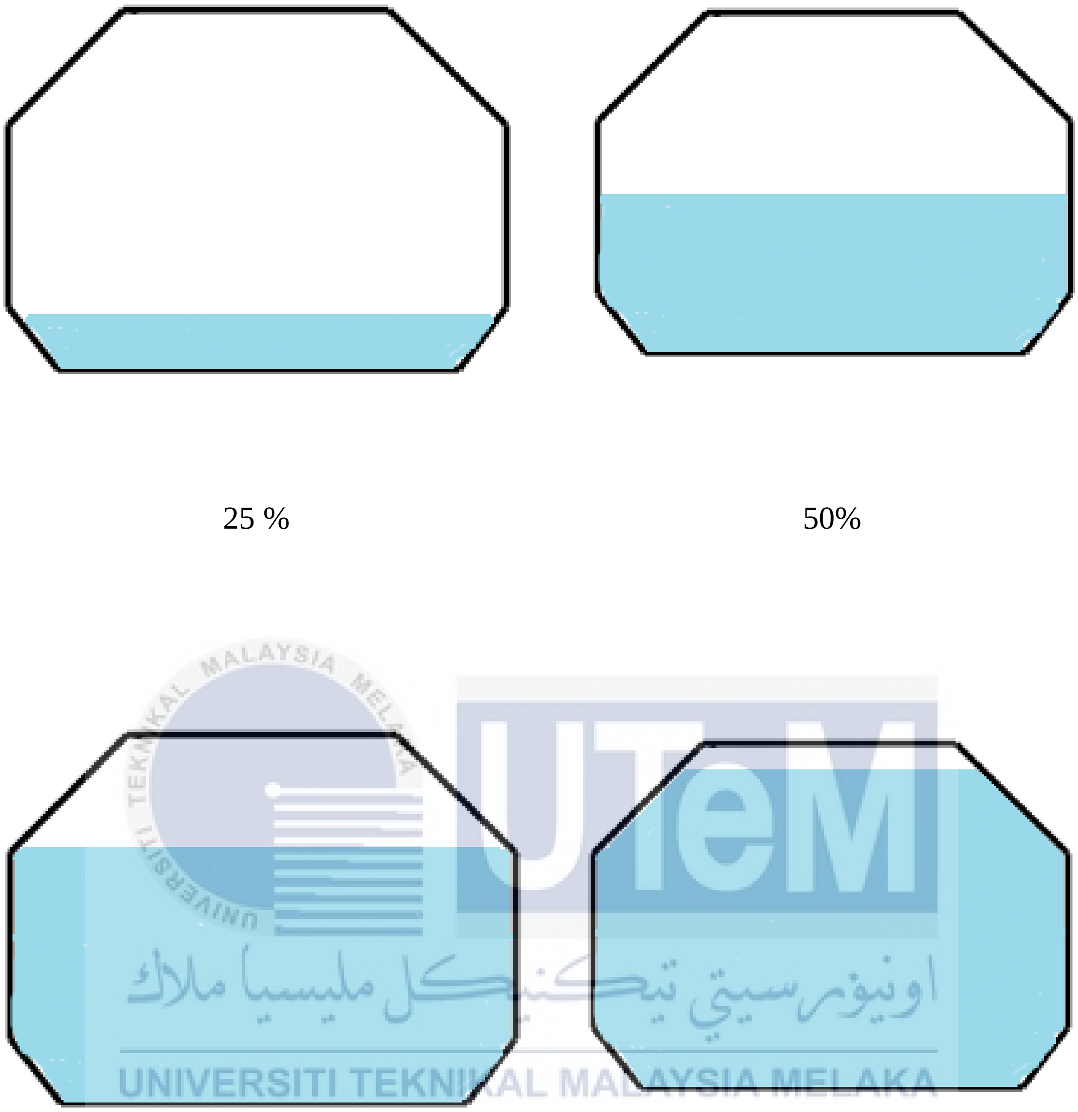

25 % 50%

75% 90%

Figure 3.10 Four different percentage of LNG level in tank

3.9.2 Types of Baffles

There are three types of baffles that will be simulate through the OpenFOAM software. The size of every baffles is same in every condition which is 1 m x 11.4 m x 12 m. For the first situation, the baffles are in horizontal which they existed on the left and right of the tank. The second condition, the baffles are in vertical where putting them at the bottom and also at the top of the tank. Lastly is the combination of the vertical and horizontal baffles condition where the baffles are at every wall of the tank. The baffle design only be tested on the filling level that the tank will experience the maximum pressure. The 2 dimensional and 3 dimensional view are shown in the Figure 3.11.

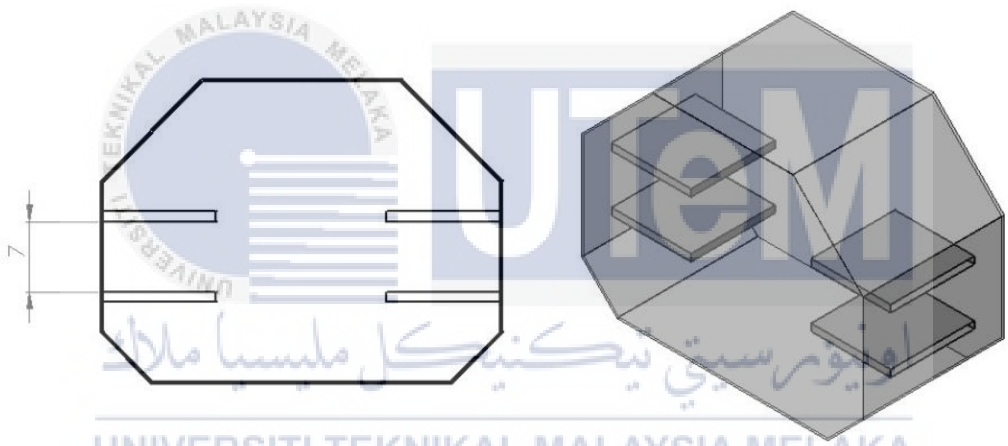

Horizontal baffles 3D of horizontal baffles

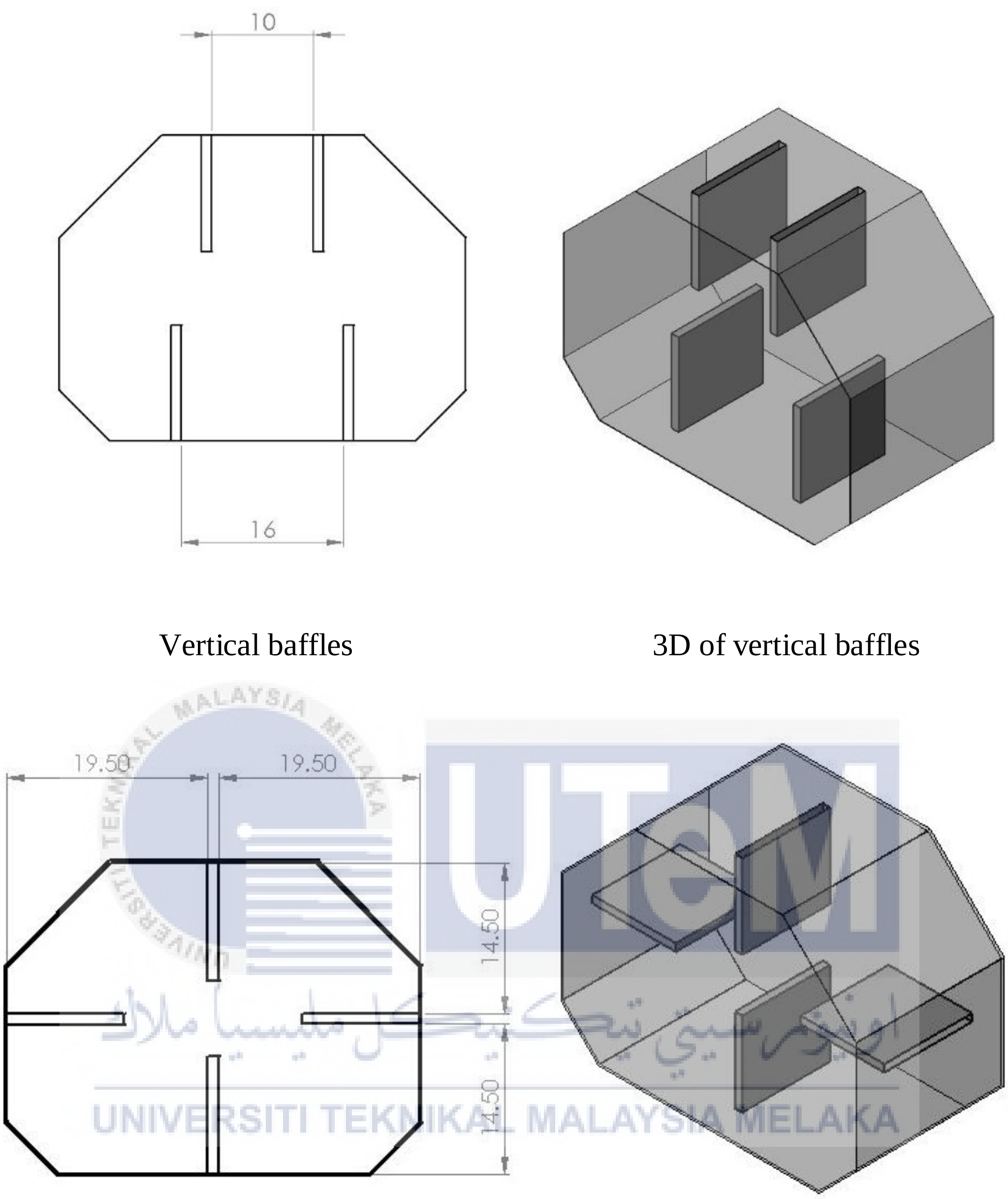

Vertical baffles — 3D of vertical baffles

Combinatorial baffles — 3D of combinatorial baffles

Figure 3.11 Types of baffles inside the LNG tank

The filling level that will obtained the maximum pressure will then simulated with three types of baffle as in Table 3.5.

Table 3.5 Case for filling level

Case	Filling Level	Baffles
1(a)	25%	Vertical baffles
1(b)	25%	Horizontal Baffles
1(c)	25%	Combined Baffles
2(a)	50%	Vertical baffles
2(b)	50%	Horizontal Baffles
2(c)	50%	Combined Baffles
3(a)	75%	Vertical baffles
3(b)	75%	Horizontal Baffles
3(c)	75%	Combined Baffles
4(a)	90%	Vertical baffles
4(b)	90%	Horizontal Baffles
4(c)	90%	Combined Baffles

3.10 Summary

To be concise, the sloshing motion of the fluid in the membrane tank is firstly simulated by using six degree of freedom where the tank moves in translation (X, Y and Z) and rotation (X', Y' and Z') direction at the same time. Then, in order to find the worst case, the tank is set to four types of filling level which are 25%, 50%, 75% and 90% from the bottom of the tank. This simulation is further carried out by performing the simulation on a tank that contain baffles to control the pressure's impact that occurred in the tank. There are three simulations because there are three types of baffles that will be conducted in this case. The first type is vertical baffles and followed by vertical baffles and combined baffles. All the simulation will be done in numerical method in OpenFOAM software by using InterFOAM features in the software.

CHAPTER 4

RESULT AND DISCUSSION

4.1 Results on each level of LNG

The simulation is tested by each of filling level which are 25%, 50%, 75% and 90% of LNG. Figure 4.1 shows the region of air and LNG in the tank while Figure 4.2 shows the pressure region of LNG and air.

Figure 4.1 Phase diagram of LNG

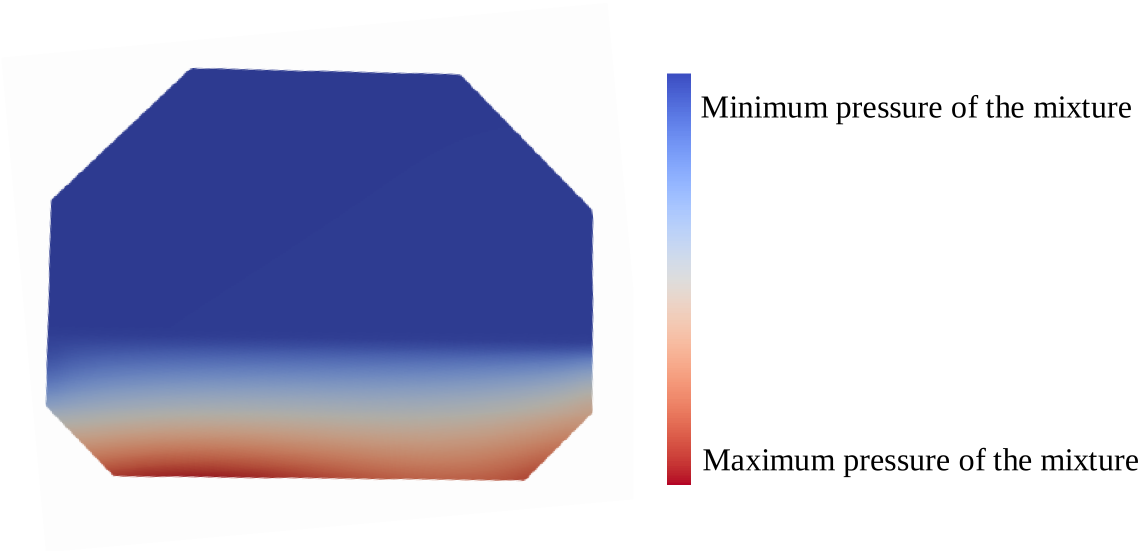

Figure 4.2 Pressure region of the mixture

4.1.1 25% of LNG

The geometry of the tank was firstly tested with the filling level of 25%. The LNG slosh in the tank when the tank moves in six-degrees of freedom. LNG splash and hit the wall of the tank. They were recorded for 40 s and the result below is the time that have been chosen as a variable on every level. Figure 4.3 until Figure 4.6 show the result of 25% of LNG in the tank.

From the Figure 4.3(a), it shows that when t = 5 s, the tank moves slightly to the right with rotation. The minimum pressure experienced in the tank is 9.39 x 10^4 Pa while the maximum pressure is 1.73 x 10^5 Pa as in Figure 4.5(a). When t = 10 s, the tank rotates to the left with 9.79 x 10^4 Pa of minimum pressure and 2.17 x 10^5 Pa of maximum pressure. The LNG splashed until it almost hit the top of the wall. After that, pressure slowly decrease when t = 15 s where the minimum pressure is 9.17 x 10^4 Pa and the maximum pressure is 1.93 x 10^5 Pa. It keep decreasing when the tank move until t = 20 s. The minimum and maximum pressure are 8.94 x 10^4 Pa and 1.68 x 10^5 Pa respectively. When t = 25 s, the maximum pressure keep decreasing until 1.61 x 10^5 and then increase when t = 30 s with 1.85 x 10^5 Pa. The condition of the pressure of LNG at t = 30 s is reduced compared to the condition of the pressure of LNG at t = 10 s. At t = 34 s and t = 40 s, the movement of LNG tank become slower as it will stop at t = 40 s. The sloshing condition become more stable than the previous time.

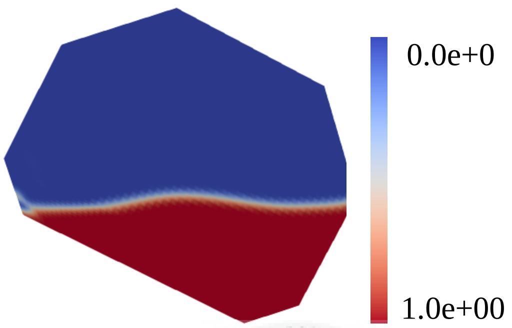

(a) Phase fraction at t = 5 s

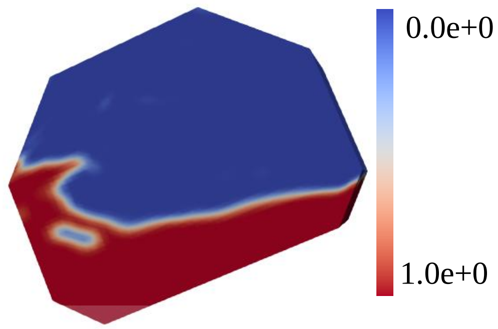

(b) Phase fraction at t = 10 s

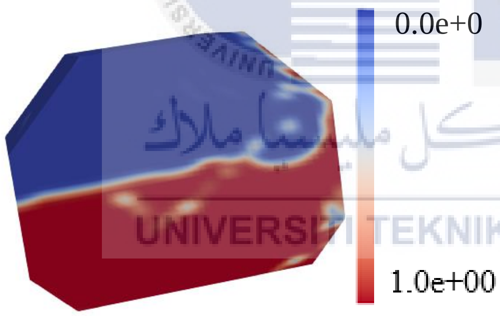

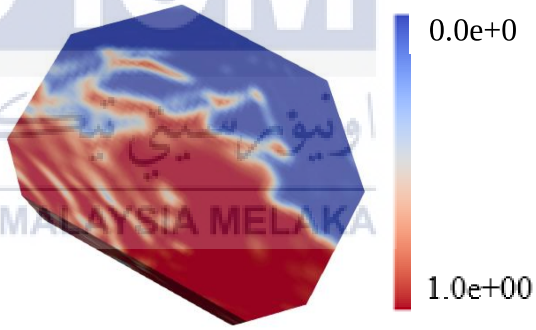

(c) Phase fraction at t = 15 s

(d) Phase fraction at t = 20 s

Figure 4.3 Phase fraction at t = 5 s until t = 20 s

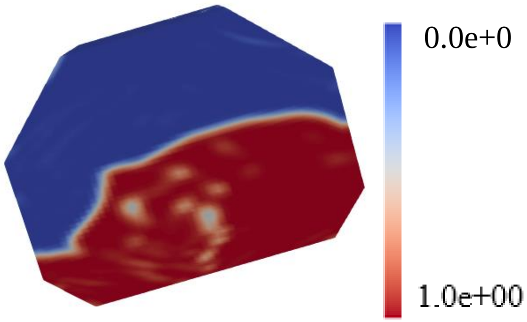

(e) Phase fraction at t = 25 s

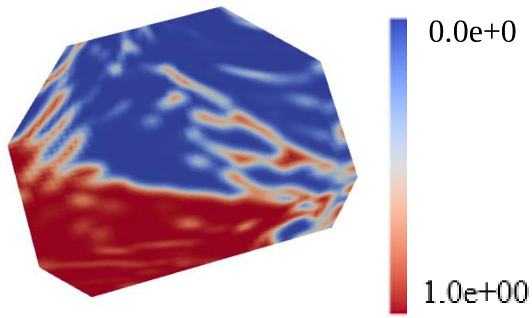

(f) Phase fraction at t = 30 s

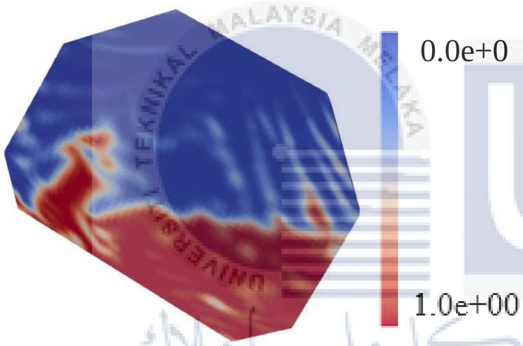

(g) Phase fraction at t = 35 s

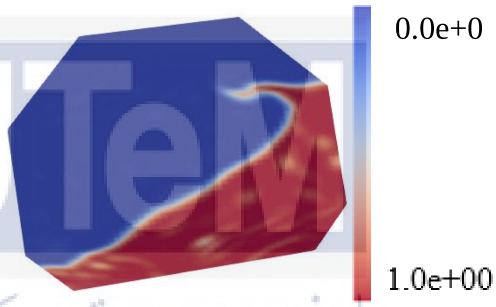

(h) Phase fraction at t = 40 s

Figure 4.4 Phase fraction at t = 25 s until t = 40 s

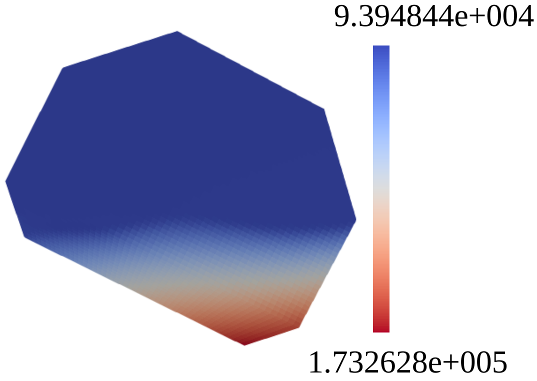

(a) Pressure at t = 5 s

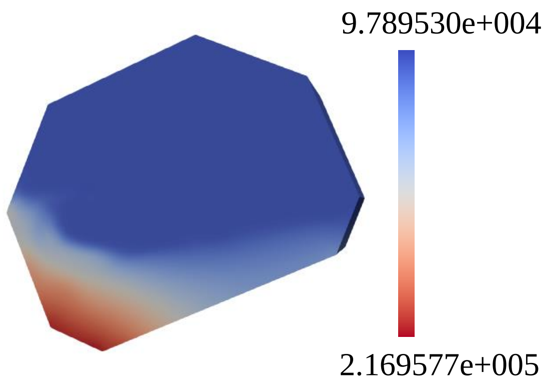

(b) Pressure at t = 10 s

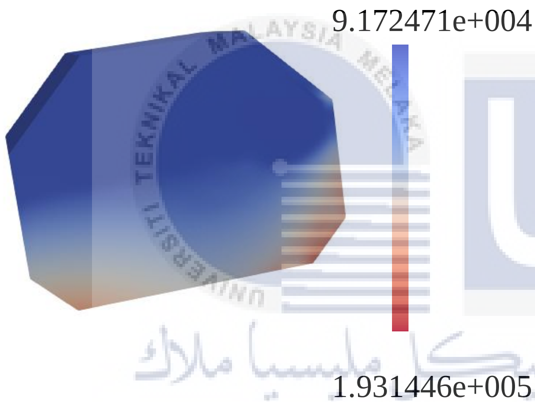

(c) Pressure at t = 15 s

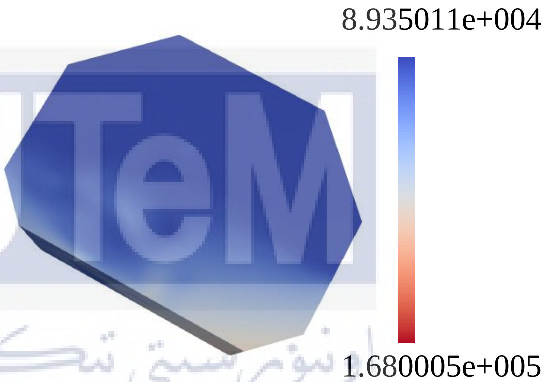

(d) Pressure at t = 20 s

Figure 4.5 Pressure at t = 5 s until t = 20 s for 25% filling level in Pa

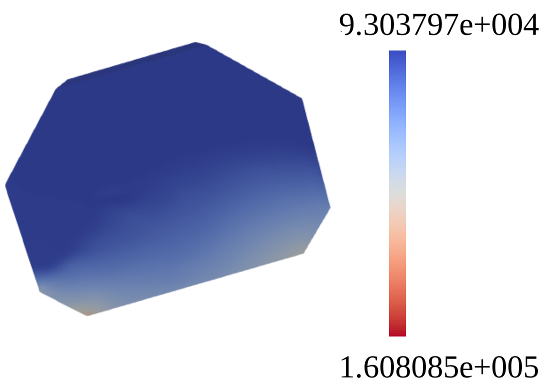

(e) Pressure at t = 25 s

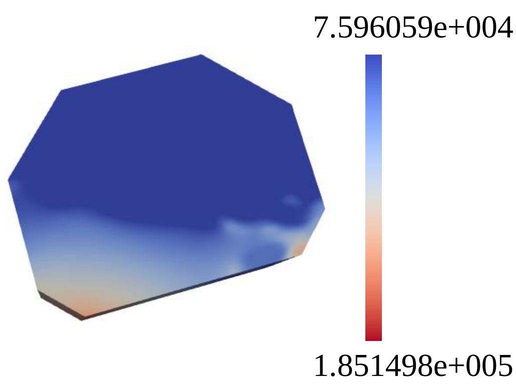

(f) Pressure at t = 30 s

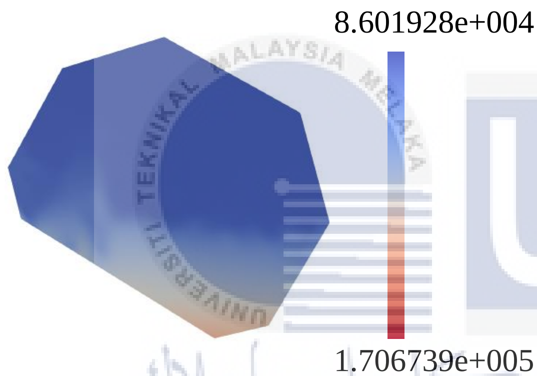

(g) Pressure at t = 35 s

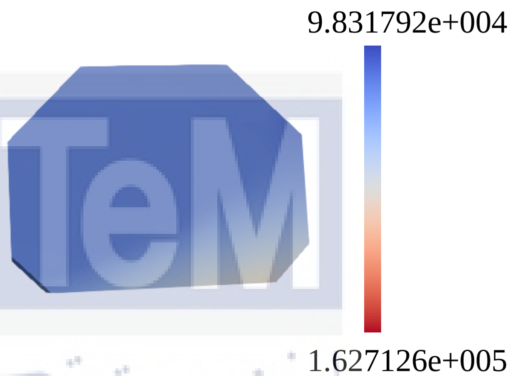

(h) Pressure at t = 40 s

Figure 4.6 Pressure at t = 25 s until t = 40 s for 25% filling level in Pa

From Figure 4.5 and Figure 4.6, the results show that maximum pressure that the tank experienced with 2.17 x 10^5 Pa is at t = 10 s as in Figure 4.7. After 10 s, the motion movement of the tank is quite stable compare to the motion at 10 s.

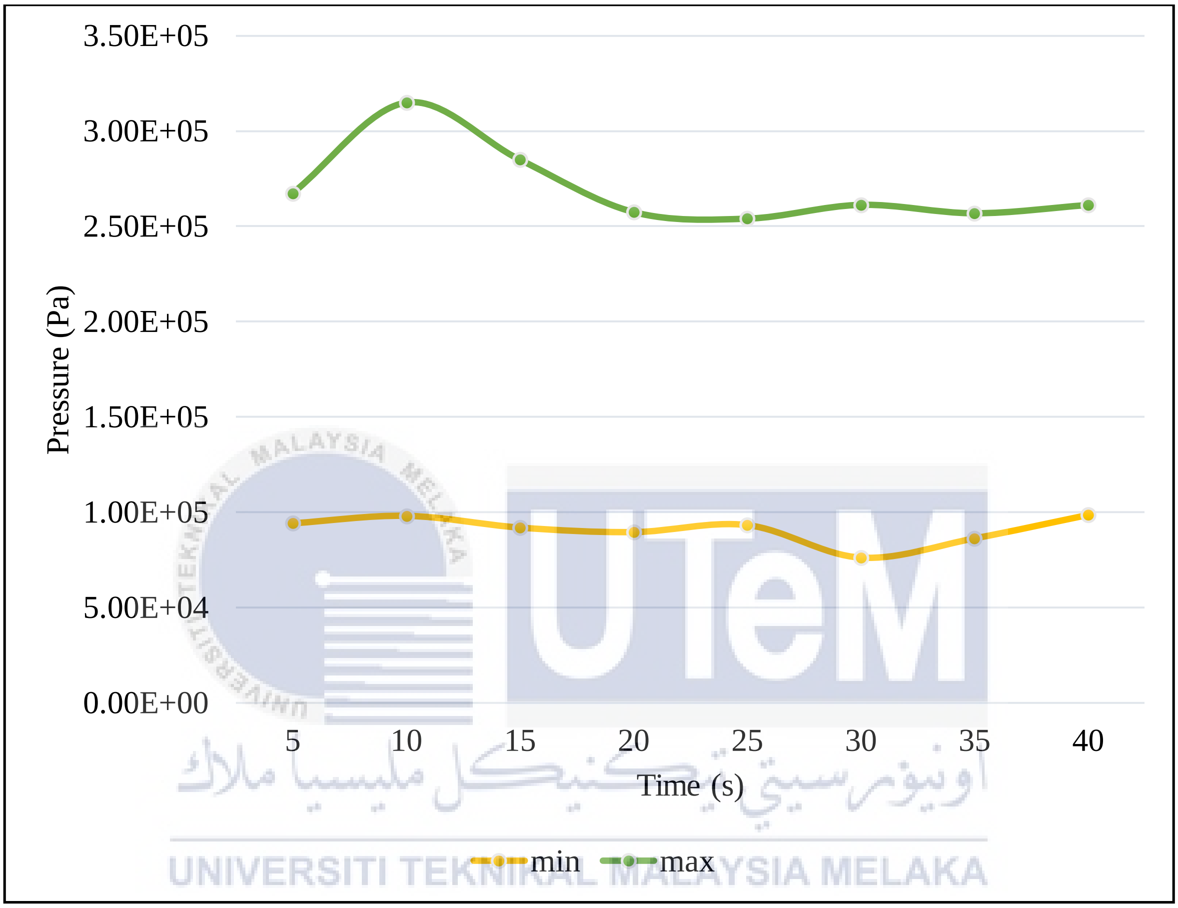

Figure 4.7 Pressure of 25% filling level of LNG against time

4.1.2 50% of LNG

The simulation of sloshing tank continue with 50% filling level of LNG. At t = 5 s, the LNG run down to the right when the tank move slightly to the right. The minimum and maximum pressure experienced by the tank are 7.68×10^4 Pa and 1.76×10^5 Pa respectively. Then, LNG run down to the left and hit the upper chamfer when t = 10 s. The minimum pressure when t = 10 s is 7.92×10^4 Pa while the maximum pressure is 2.10×10^5 Pa. In 50% of LNG in the tank, the maximum pressure that the tank experienced is when t = 10 s compares to another seconds. Then, when t = 15 s, the LNG now mostly at the bottom of the tank with minimum and maximum pressure are 8.05×10^4 Pa and 1.75×10^5 Pa respectively. After that, the LNG run down to the left of the tank at t = 20 s and experienced 8.31×10^4 Pa as a minimum pressure and 1.71×10^5 Pa as maximum pressure. The minimum pressure increase when t = 25 s with 7.10×10^4 Pa while the maximum pressure also with 1.84×10^5 Pa. when t = 30 s, the pressure slightly decrease with minimum and maximum pressure at 6.75×10^4 Pa and 1.83×10^5 Pa. When t = 35 s and t = 40 s, the pressure keep decreasing until the maximum pressure are 1.74×10^5 Pa and 1.68×10^5 Pa respectively.

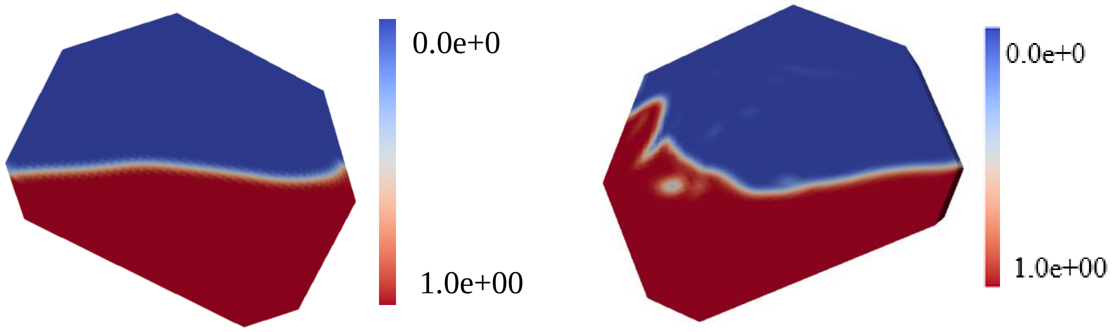

(a) Phase fraction at t = 5 s (b) Phase fraction at t = 10 s

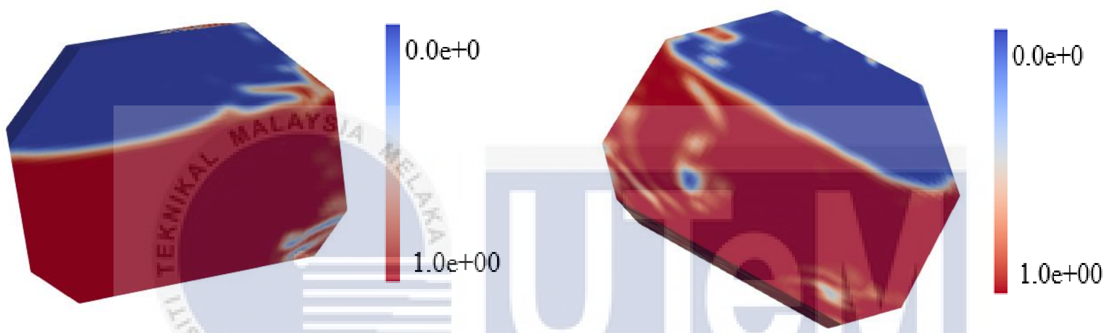

(c) Phase fraction at t = 15 s (d) Phase fraction at t = 20 s

Figure 4.8 Phase fraction at t = 5 s until t = 20 s

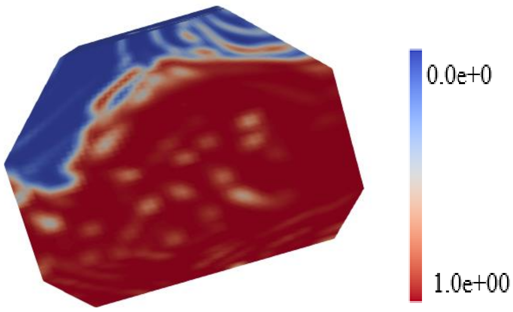

(e) Phase fraction at t = 25 s

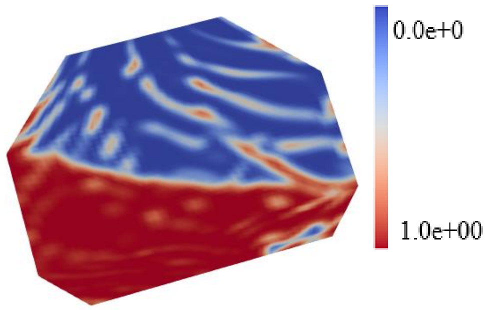

(f) Phase fraction at t = 30 s

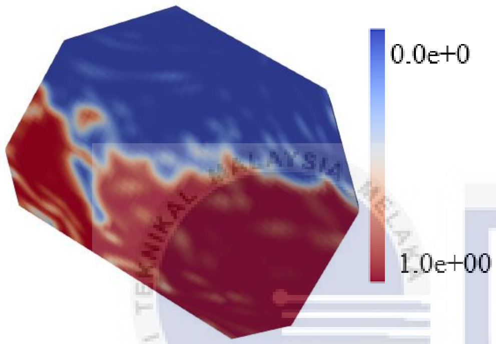

(g) Phase fraction at t = 35 s

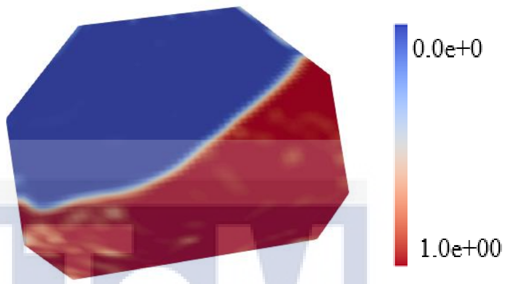

(h) Phase fraction at t = 40 s

Figure 4. 9 Phase fraction at t = 25 s until t = 40 s

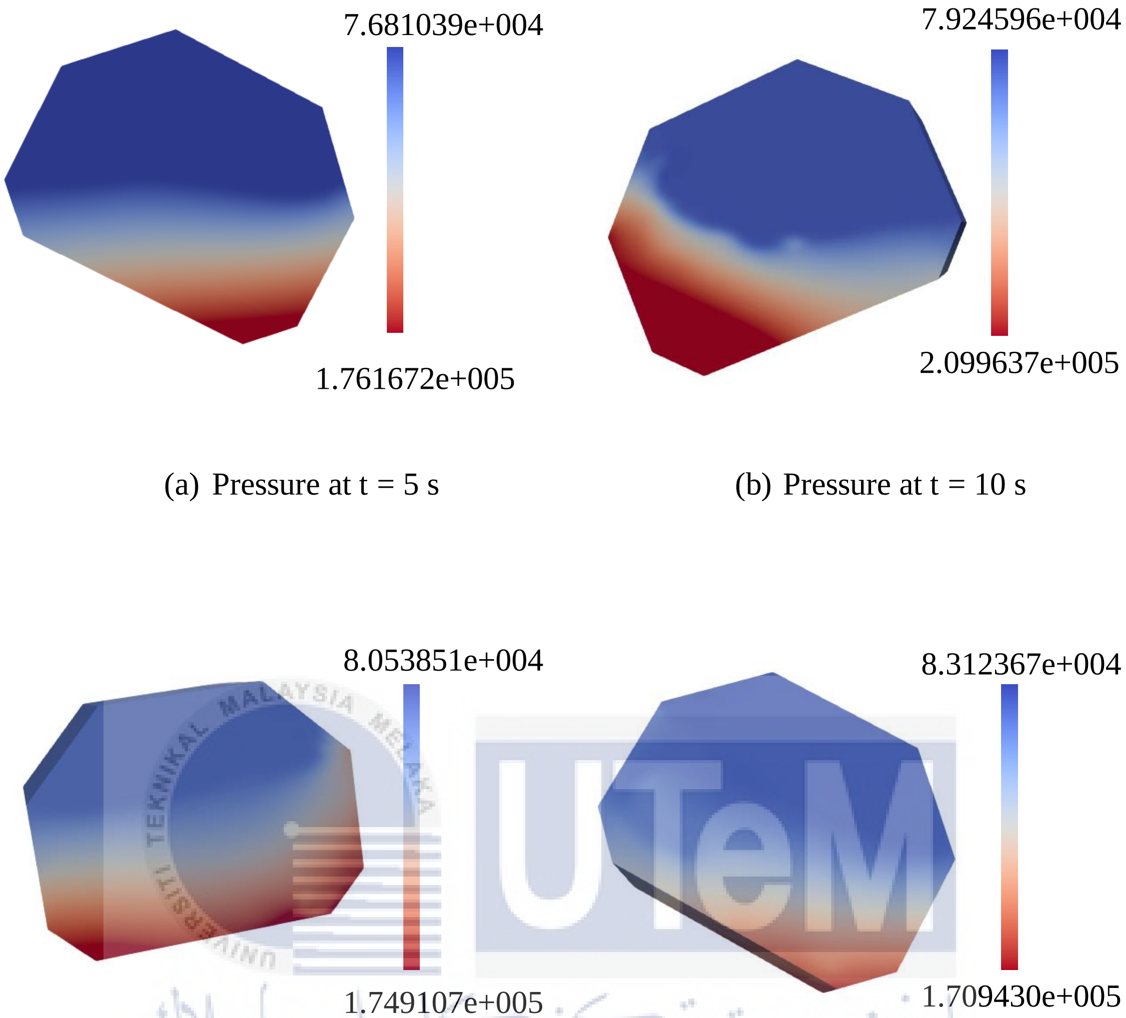

(a) Pressure at t = 5 s (b) Pressure at t = 10 s

(c) Pressure at t = 15 s (d) Pressure at t = 20 s

Figure 4.10 Pressure at t = 5 s until t = 20 s for 50% filling level in Pa

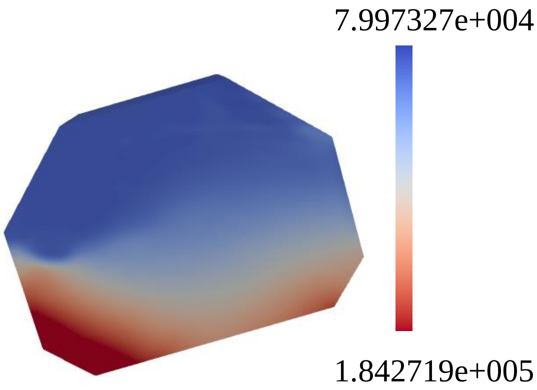

(e) Pressure at t = 25 s

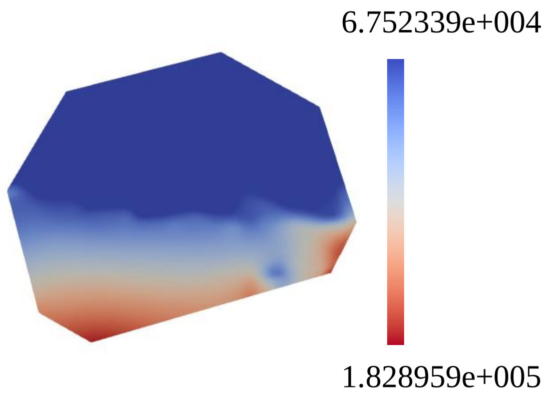

(f) Pressure at t = 30 s

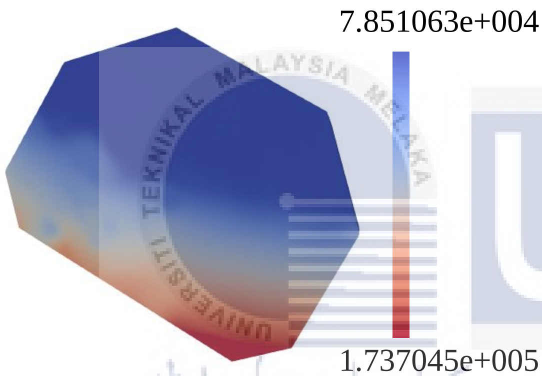

(g) Pressure at t = 35 s

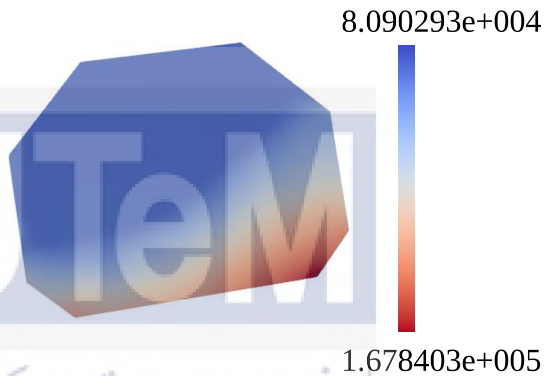

(h) Pressure at t = 40 s

Figure 4.11 Pressure at t = 25 s until t = 40 s for 50% filling level in Pa

From Figure 4.10 and Figure 4.11, it shows that the tank experienced the minimum pressure with 6.75 x 10^4 Pa at t = 30 s while the maximum pressure with 2.10 x 10^5 Pa at t = 10 s. The whole results shows in Figure 4.12 below.

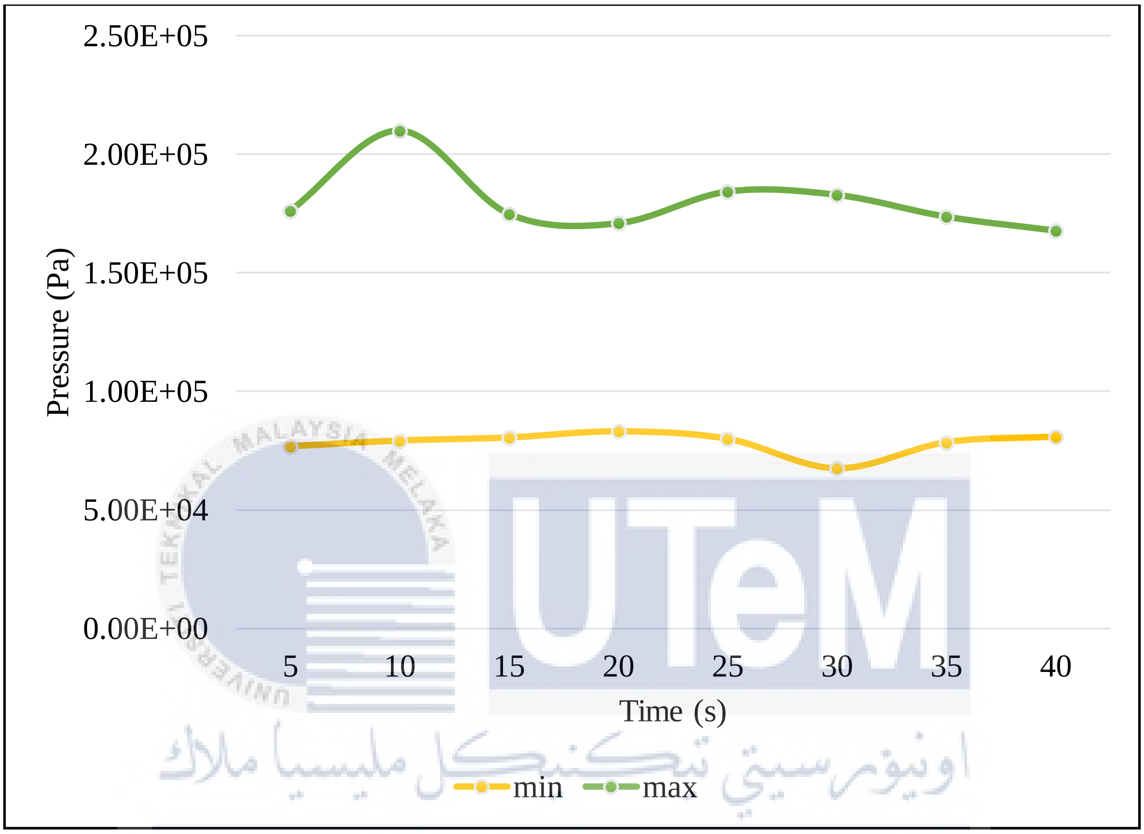

Figure 4.12 Pressure of 50% filling level of LNG against time

4.1.3 75% of LNG

In the tank of 75% of LNG, the filling level is more than a half of the tank. The sloshing phenomenon occurred with lesser impact of pressure compared to 50% of filling level of LNG. As from the Figure 4.13, when t = 5 s, the movement of LNG still in a steady condition with minimum pressure that the tank experienced is 4.59×10^4 Pa while maximum pressure is 1.79×10^5 Pa. Once the tank is at t = 10 s, the LNG splashed until hit the top of the tank with the minimum pressure of 3.54×10^4 Pa and maximum pressure of 2.63×10^5 Pa. After that, the maximum pressure decrease when t = 15 s with 1.60×10^5 Pa while the minimum pressure increase until 4.78×10^4 Pa. When t = 20 s, minimum and maximum pressure are slightly increase to 4.81×10^4 Pa and 1.78×10^5 Pa respectively. The tank experienced 3.40×10^4 Pa of minimum pressure and 1.99×10^5 Pa of maximum pressure at t = 25 s. Then, when t = 30 s, minimum pressure increase to 3.84×10^4 Pa and maximum pressure decrease to 1.70×10^5 Pa. The condition of pressure keep decreasing until t = 40 s with minimum pressure of 4.37×10^4 Pa and maximum pressure of 1.53×10^5 Pa.

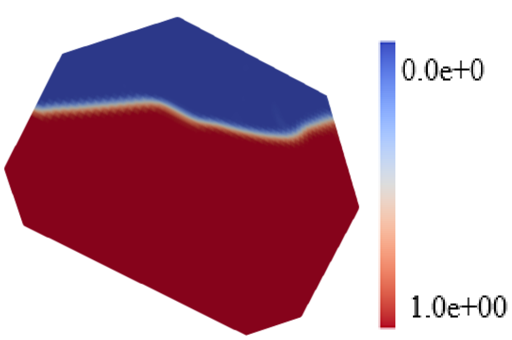

(a) Phase fraction at t = 5 s

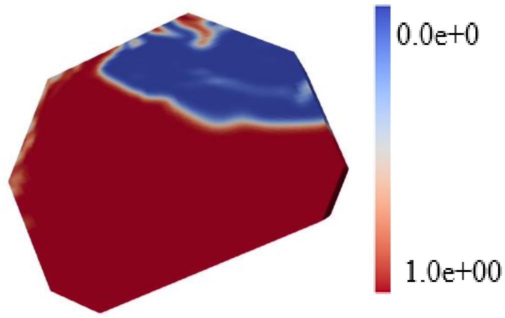

(b) Phase fraction at t = 10 s

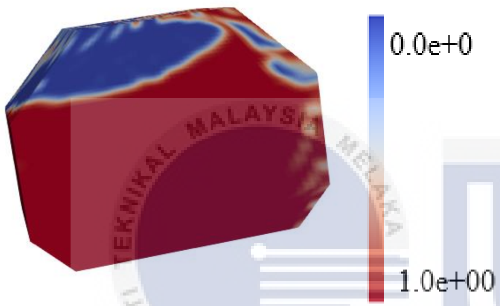

(c) Phase fraction at t = 15 s

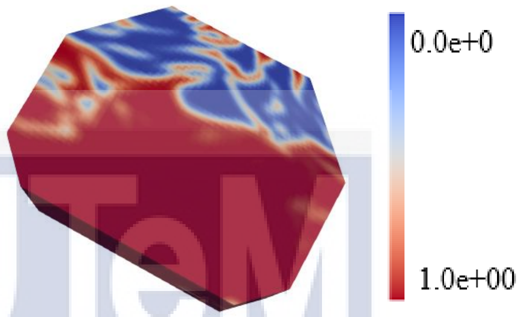

(d) Phase fraction at t = 20 s

Figure 4.13 Phase fraction at t = 5 s until t =20 s

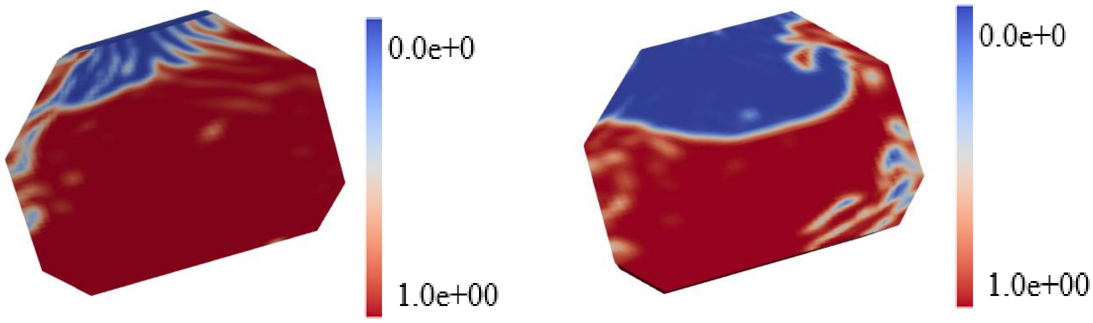

(e) Phase fraction at t = 25 s

(f) Phase fraction at t = 30 s

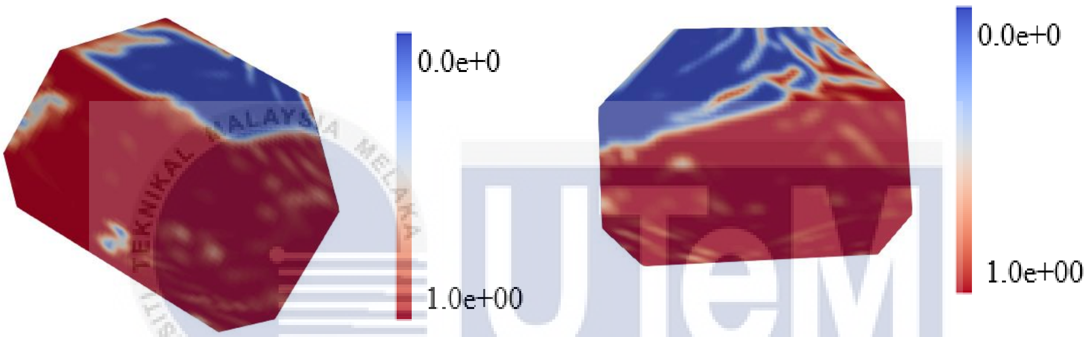

(g) Phase fraction at t = 35 s

(h) Phase fraction at t = 40 s

Figure 4.14 Phase fraction at t = 25 s until 40 s

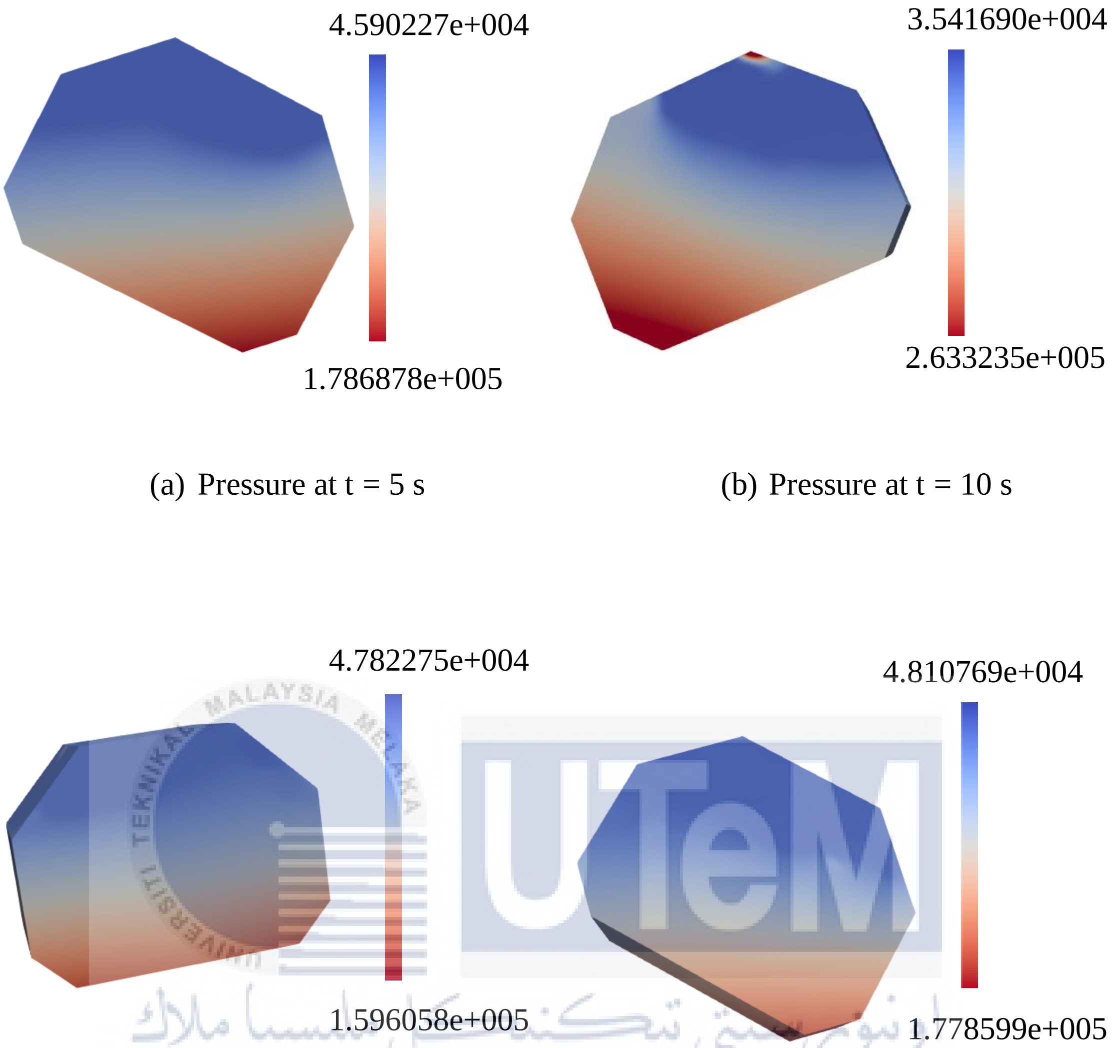

(a) Pressure at t = 5 s

(b) Pressure at t = 10 s

(c) Pressure at t = 15 s

(d) Pressure at t = 20 s

Figure 4.15 Pressure at t = 5 s until t = 20 s for 75% filling level in Pa

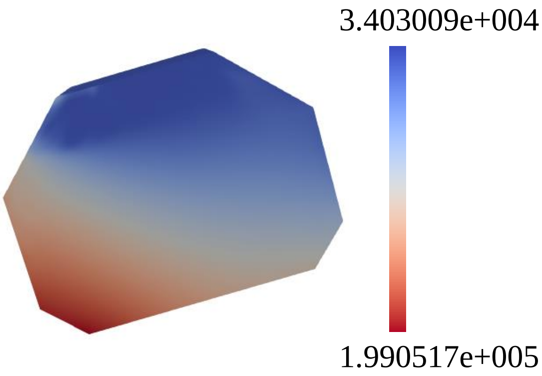

(e) Pressure at t = 25 s

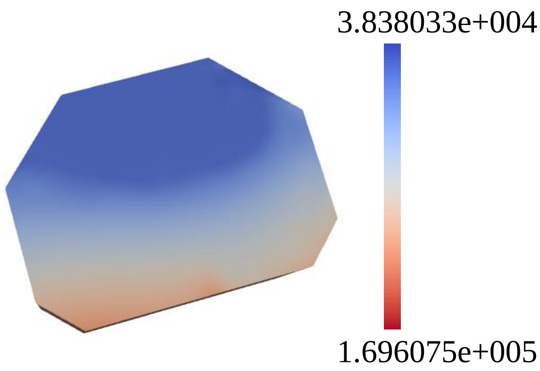

(f) Pressure at t = 30 s

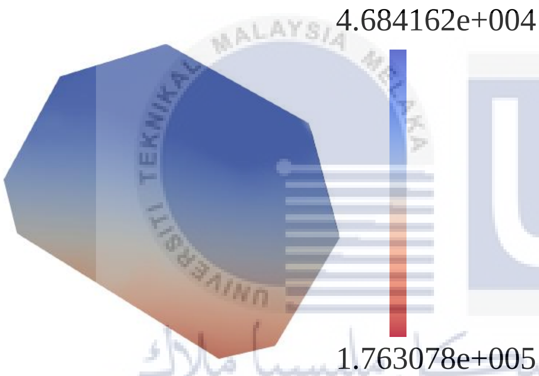

(g) Pressure at t = 35 s

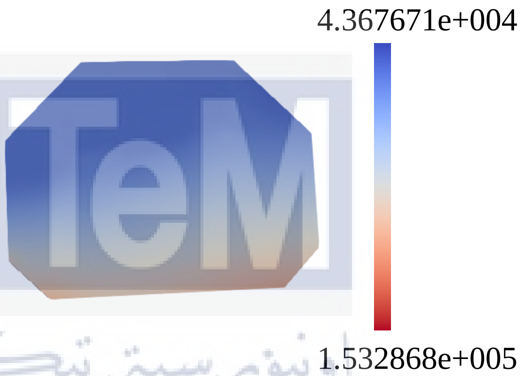

(h) Pressure at t = 40 s

Figure 4.16 Pressure at t = 25 s until t = 40 s for 75% filling level in Pa

In this level, there is the highest maximum pressure occurred at t = 10 s with 2.63 x 10^5 Pa while at t = 40 s, the tank does not slosh violently. The comparison is in Figure 4.17.

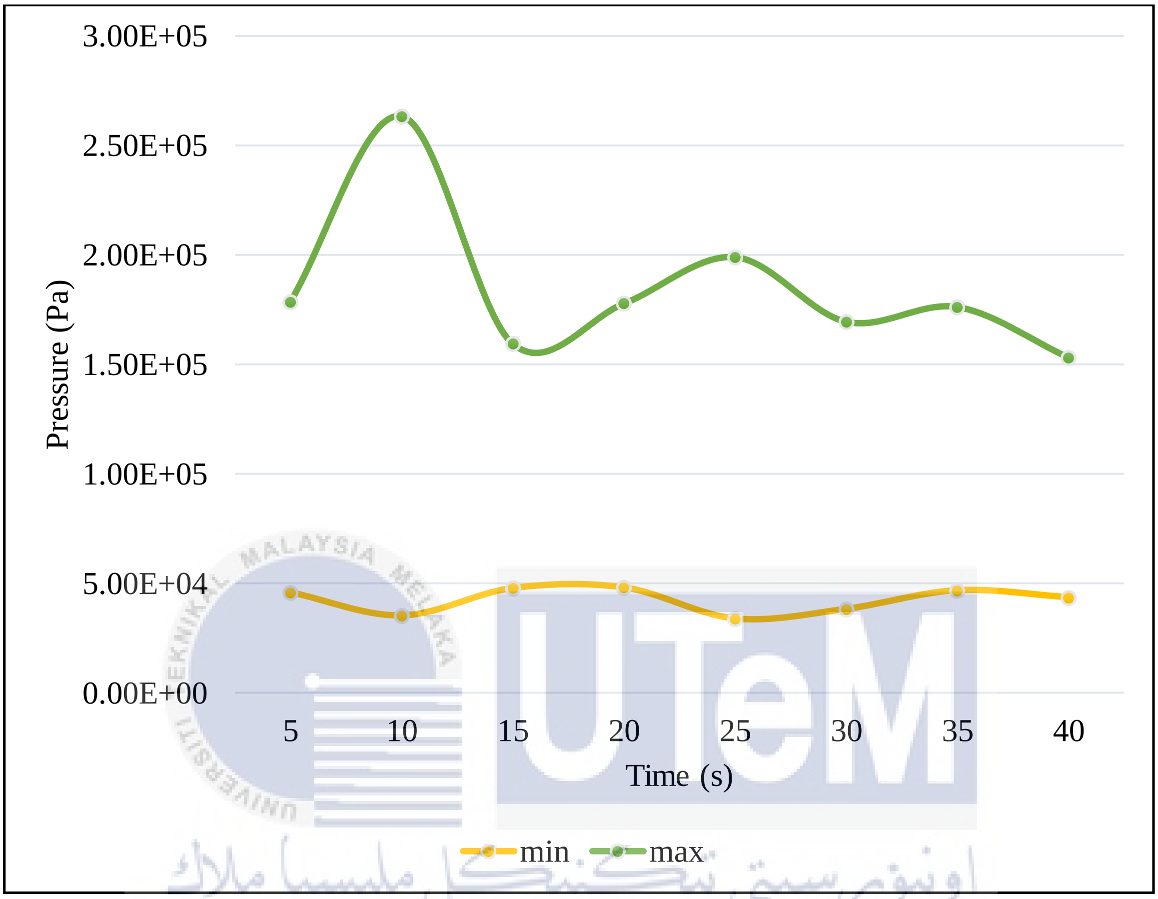

Figure 4.17 Pressure of 75% filling level of LNG against time

4.1.4 90% of LNG

In this level, the LNG almost occupied the tank with only 10% of air. As in the Figure 4.18, it shows time at 5 s and 10 s. When t = 5s, the tank slightly rotate to the right and maximum pressure occurred at the right bottom of the tank with 1.82 x 10^5 Pa. While at t = 10 s, maximum pressure occurred at the left bottom of the tank when the tank slightly rotate to the left. The part that experienced the maximum pressure is caused by the part need to bear with the load of LNG. The tank then experienced the maximum pressure of 1.59 x 10^5 Pa and minimum pressure of 2.29 x 10^4 Pa at t = 15 s. After that, both minimum pressure and maximum pressure increase with 2.45 x 10^4 Pa and 1.84 x 10^5 Pa respectively at t = 20 s. At t = 25 s, the tank experienced the highest maximum pressure compare to the other time. The maximum pressure is 1.91 x 10^5 Pa and minimum pressure is 1.02 x 10^4 Pa. After that, the maximum pressure keep decreasing from t = 30 s until t = 40 s.

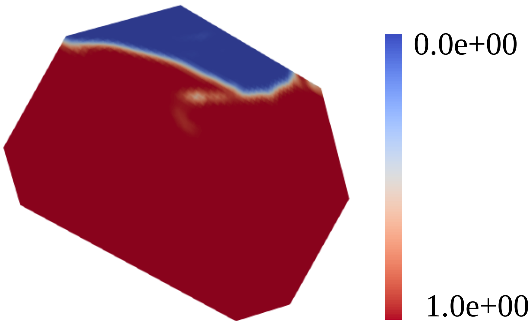

(a) Phase fraction at t = 5 s

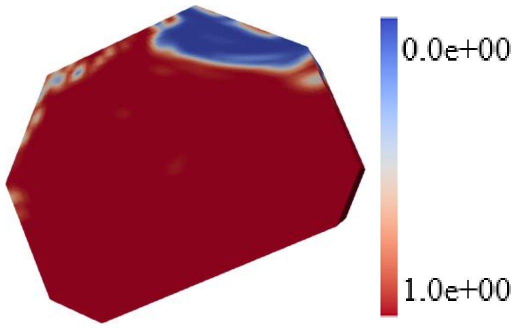

(b) Phase fraction at t = 10 s

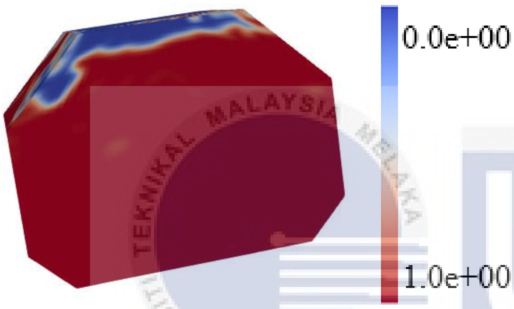

(c) Phase fraction at t = 15 s

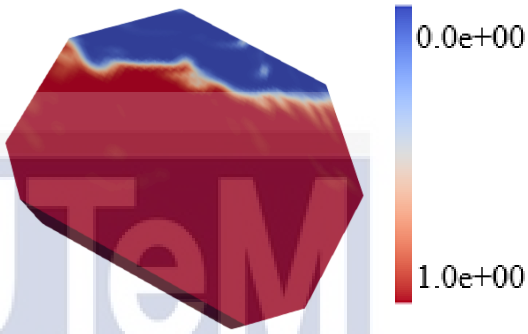

(d) Phase fraction at t = 20 s

Figure 4.18 Phase fraction at t = 5 s until t = 20 s

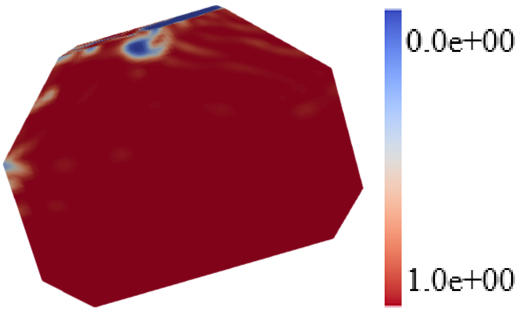

(e) Phase fraction at t = 25 s

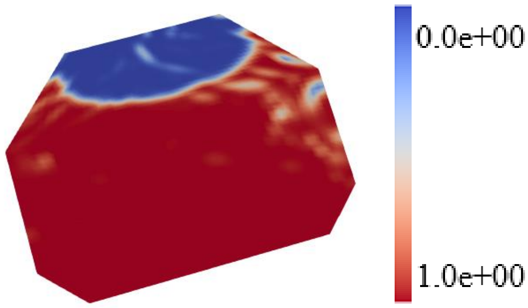

(f) Phase fraction at t = 30 s

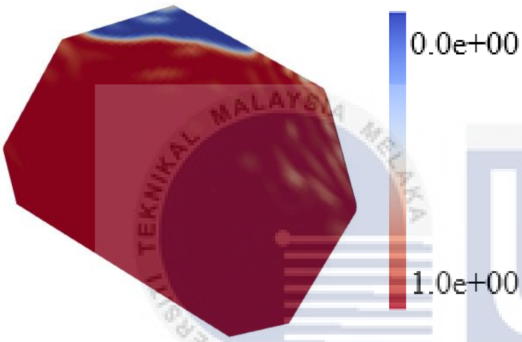

(g) Phase fraction at t = 35 s

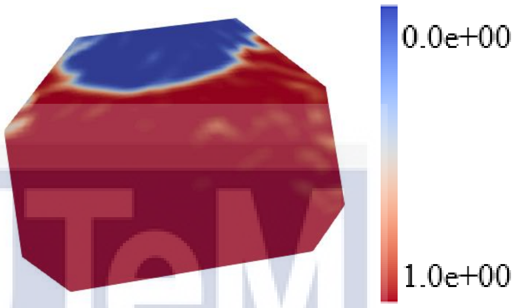

(h) Phase fraction at t = 40 s

Figure 4.19 Phase fraction at t = 25 s until t = 40 s

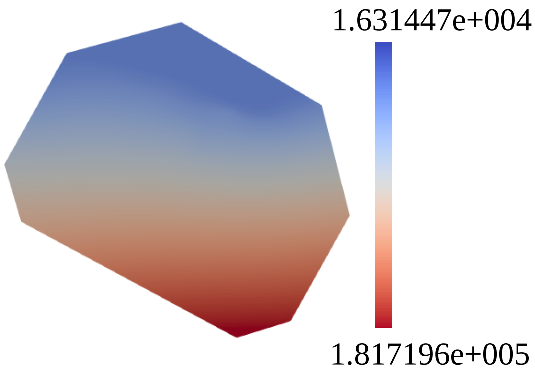

(a) Pressure at t = 5 s

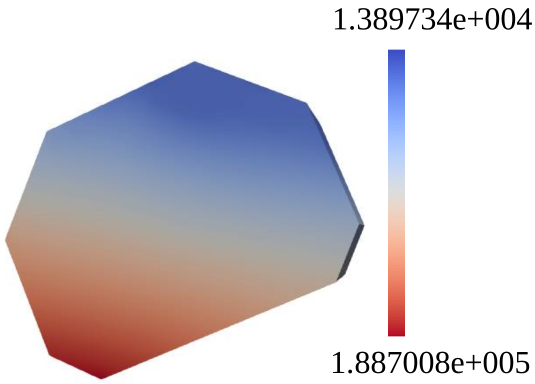

(b) Pressure at t = 10 s

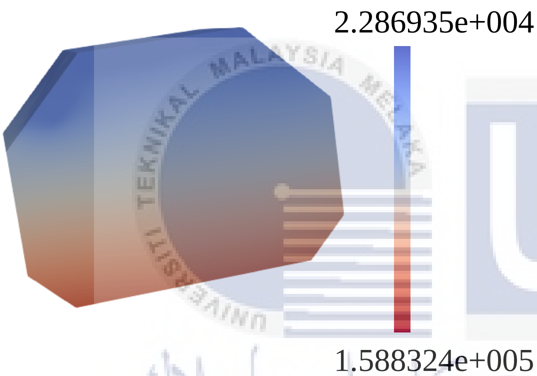

(c) Pressure at t = 15 s

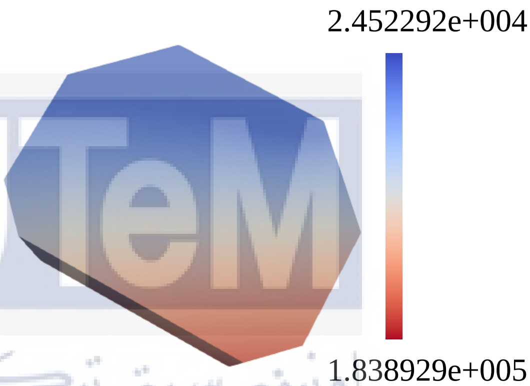

(d) Pressure at t = 20 s

Figure 4.20 Pressure at t = 5 s until t = 20 s for 90% filling level in Pa

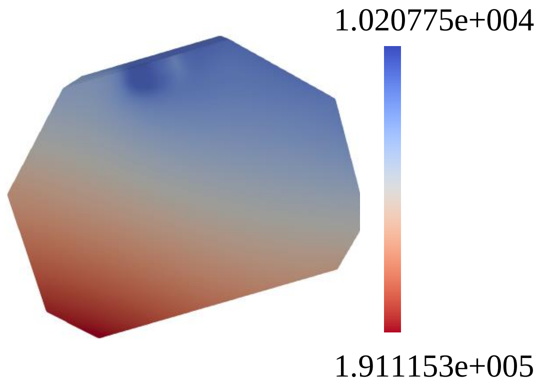

(e) Pressure at t = 25 s

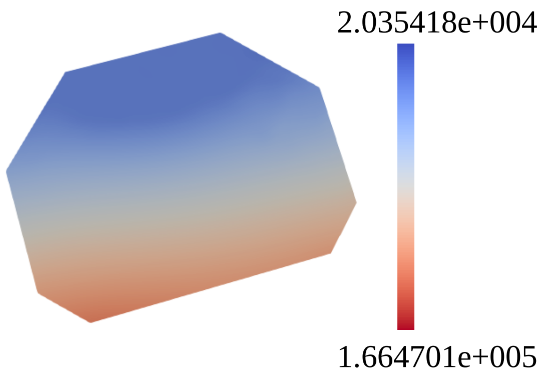

(f) Pressure at t = 30 s

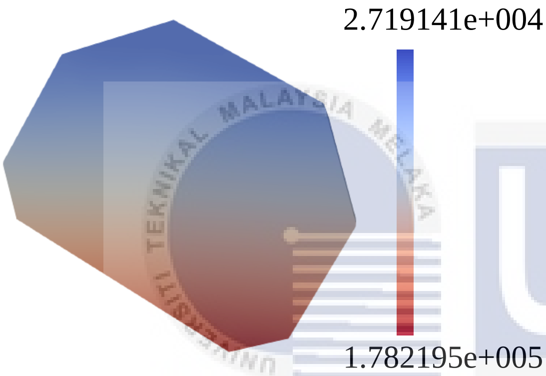

(g) Pressure at t = 35 s

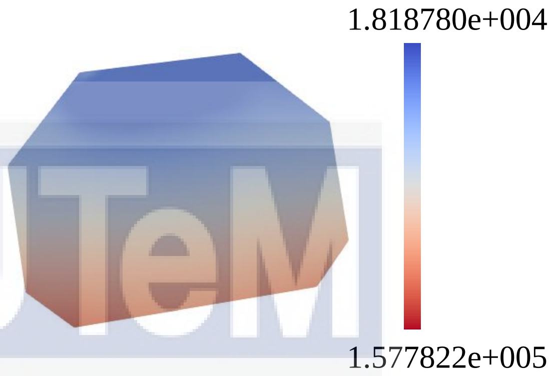

(h) Pressure at t = 40 s

Figure 4.21 Pressure at t = 25 s until t = 40 s for 90% filling level in Pa

The difference between minimum and maximum pressure in this filling level is quite different because of the filling level is almost filled up the tank. We can see the average pressure on this level is quite high as in Figure 4.22.

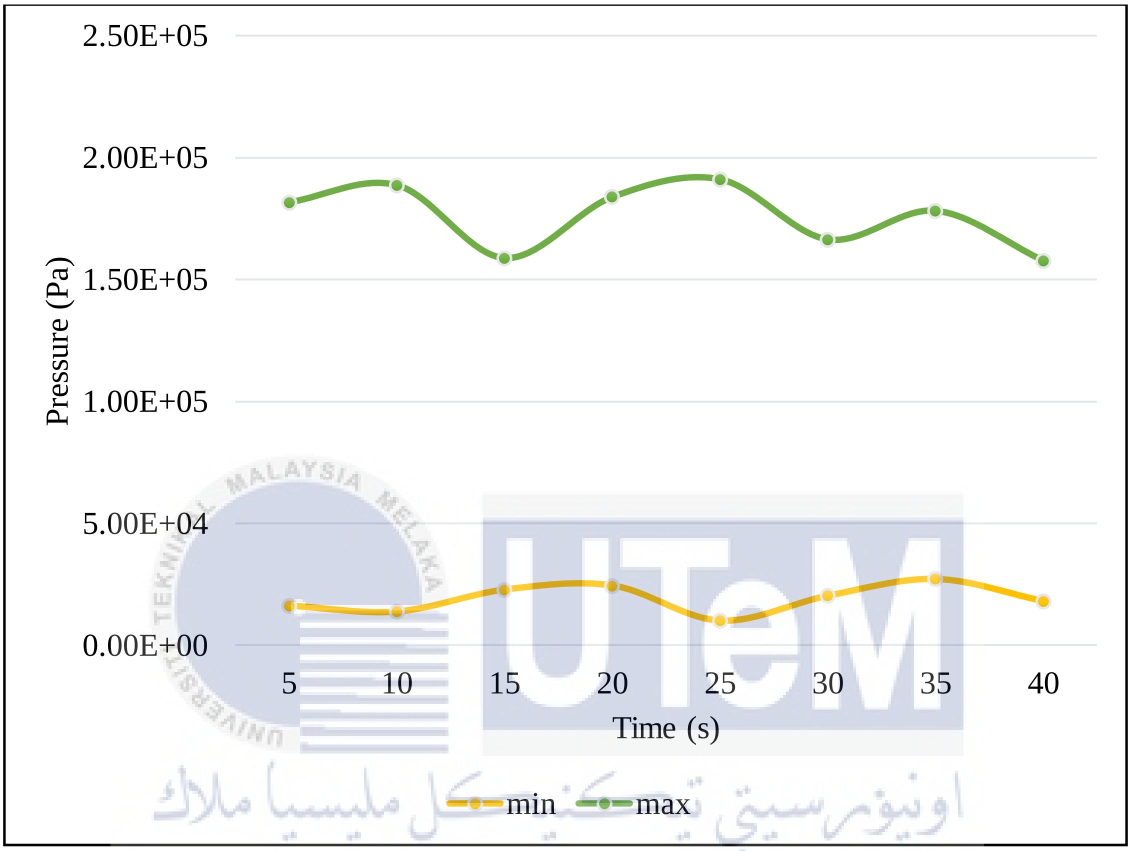

Figure 4.22 Pressure of 90% filling level of LNG against time

4.2 Comparison of sloshing motion with previous study

Based on Figure 4.3(b), the LNG motion at t = 10 s of 25% filling level of LNG can be seen quite similar to the motion from journal Wei Wang et al (2014) when the LNG running down to the left and almost hit the upper left chamfer as in Figure 4.23.

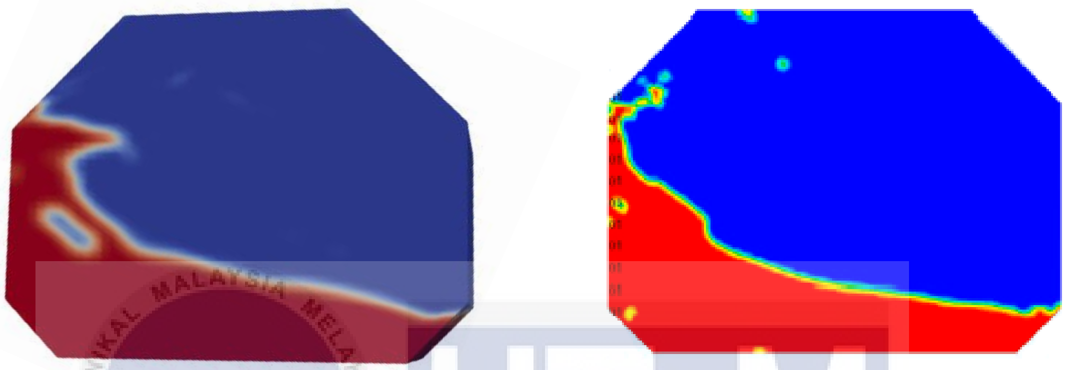

(a) Present result (b) Wei Wang et al (2014)

Figure 4.23 Phase fraction of present result and Wei Wang et al (2014) at t = 10 s of 25% LNG

In 50% filling level of LNG at t = 10 s, the phase fraction also can be seen quite similar to the Wei Wang et al (2014) as in Figure 4.24.

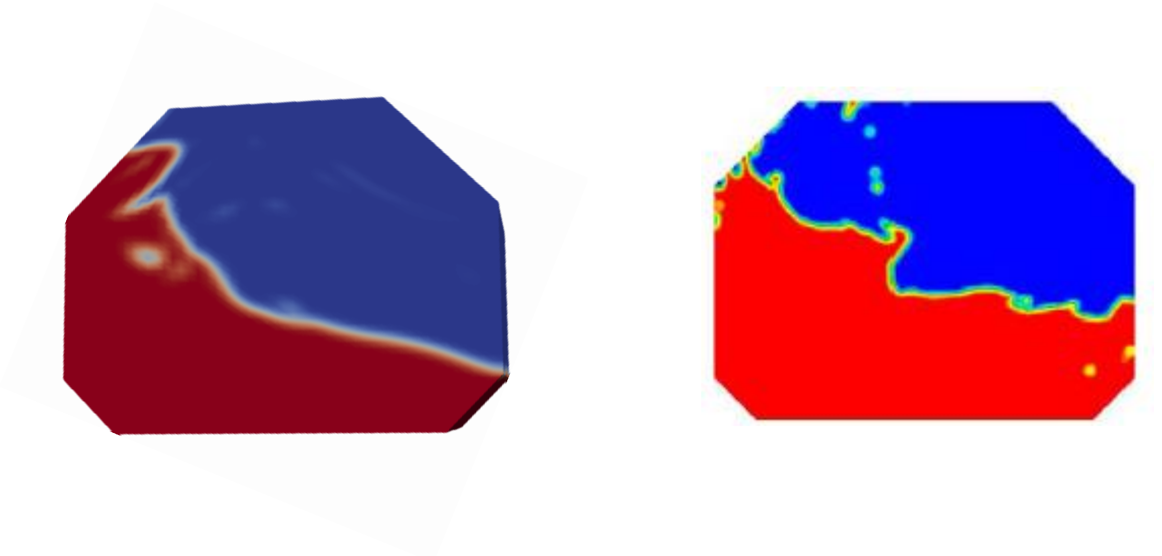

(a) Present result (b) Wei Wang et al (2014)

Figure 4.24 Phase fraction of present result and Wei Wang et al (2014) at t = 10 s of 50% of LNG

However, there is a slight different in term of motion direction of LNG in 75% filling of LNG where the LNG splashed at the left side of the tank compared to the previous study which showed a different splash motion as in Figure 4.25.

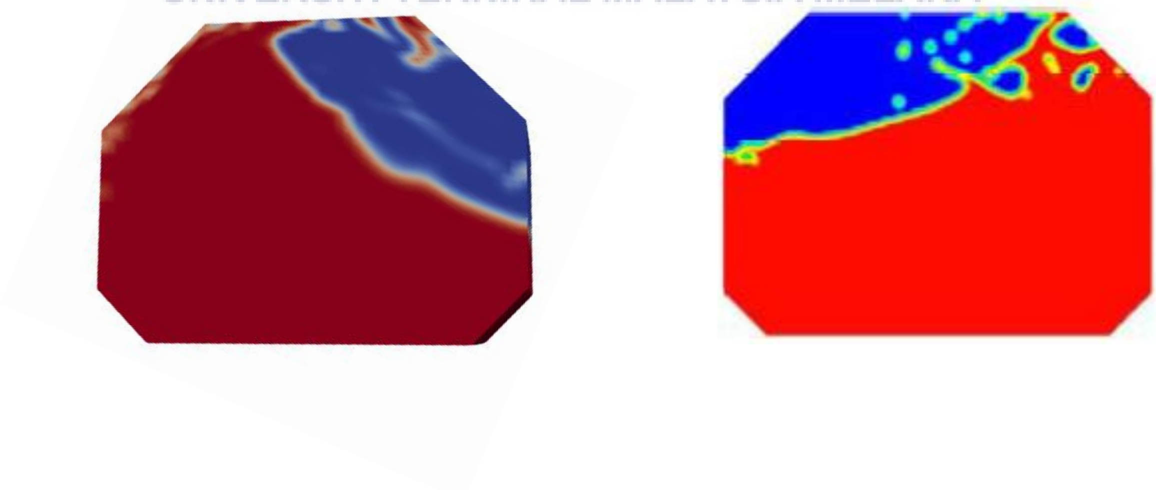

(a) Present result (b) Wei Wang et al (2014)

Figure 4.25 Phase fraction of present result and Wei Wang et al (2014) at t = 10 s of 75% of LNG

4.3 Comparison between all filling levels

Figure below shows the comparison of maximum pressure between all filling levels of LNG. From the Figure 4.26, 75% filling level of LNG experienced the highest maximum pressure at t = 10 s, but it also experienced the least maximum pressure at t = 40 s. By this rate, the tank itself can lead to cracks due to excessive pressure.

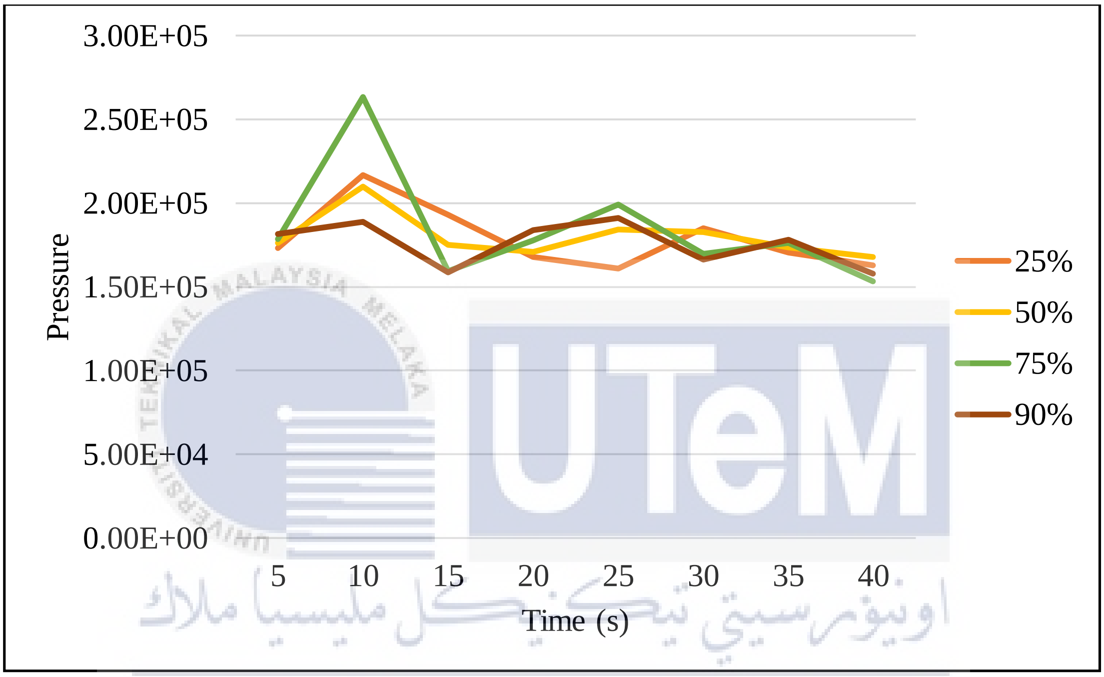

Figure 4.26 Pressure of each filling level of LNG against time

4.4 Baffles

The filling level that obtained highest maximum pressure is 75% of LNG. Thus, the simulations of every type of baffles been simulated by testing the 75% filling level of LNG.

4.4.1 Horizontal baffles

From the Figures 4.27 below. It shows that the highest maximum pressure is when t = 10 s with 1.92 x 10^5 Pa. With the comparison from no baffle tank, the pressure is reduce from 2.63 x 10^5 Pa. Not only the observation from maximum pressure, but minimum pressure also reduce from 4.81 x 10^4 Pa to 4.69 x 10^4 Pa at t = 25 s to t = 35 s. The sloshing diagrams shown in Figure 4.28 until Figure 4.31.

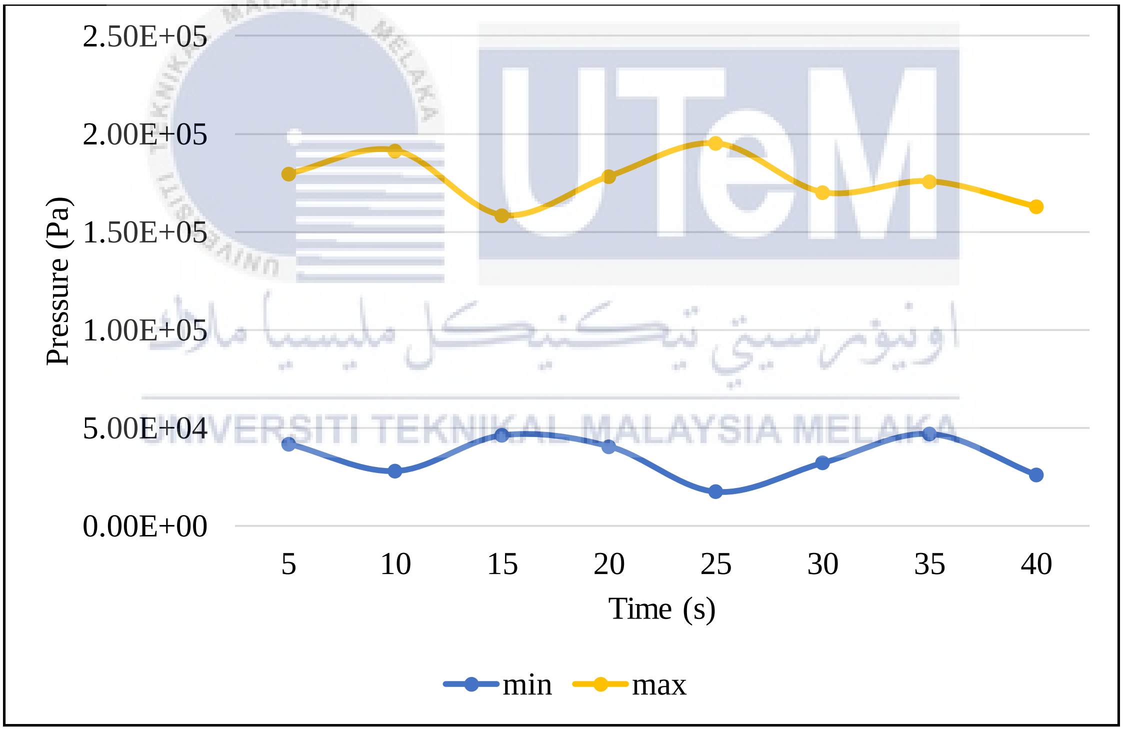

Figure 4.27 Pressure of LNG with horizontal baffles against time

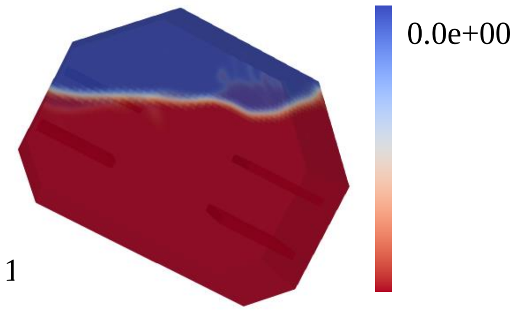

(a) Phase fraction at t = 5 s

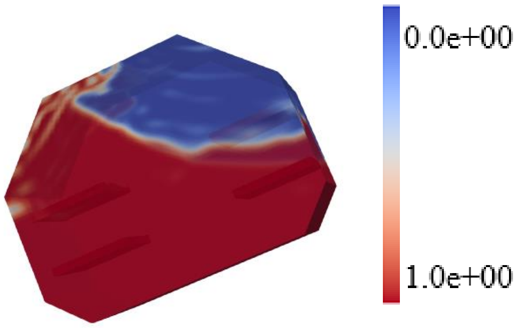

(b) Phase fraction at t = 10 s

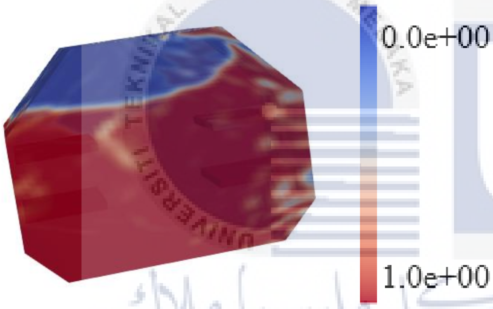

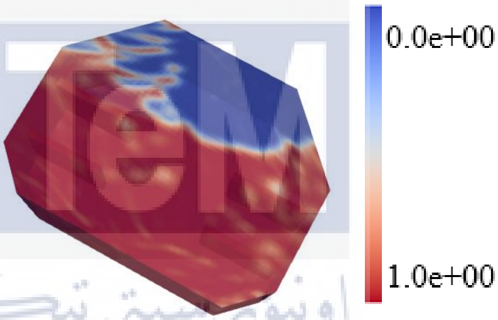

(c) Phase fraction at t = 15 s

(d) Phase fraction at t = 20 s

Figure 4.28 Phase fraction at t = 5 s until t = 20 s

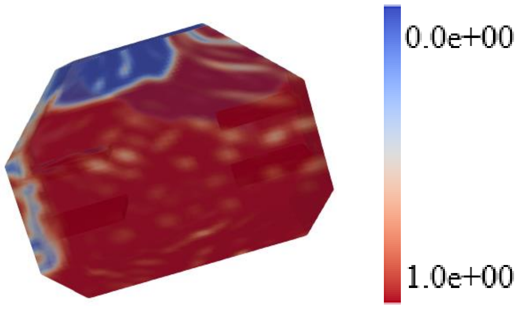

(e) Phase fraction at t = 25 s

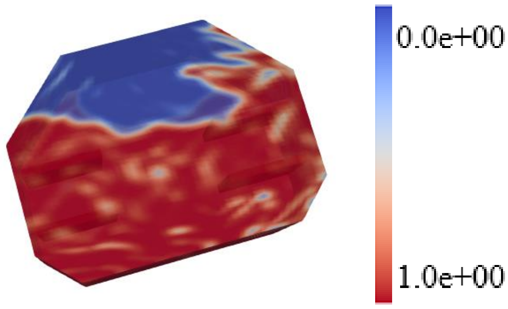

(f) Phase fraction at t = 30 s

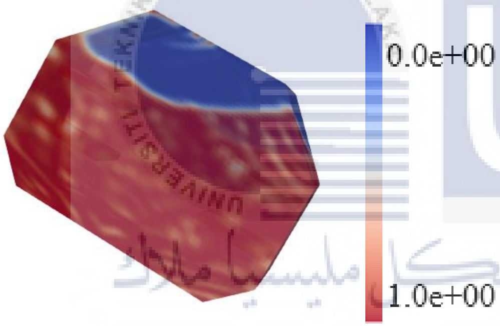

(g) Phase fraction at t = 35 s

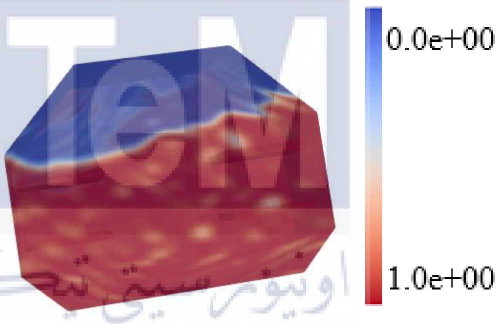

(h) Phase fraction at t = 40 s

Figure 4.29 Phase fraction at t = 25 s until t = 40 s

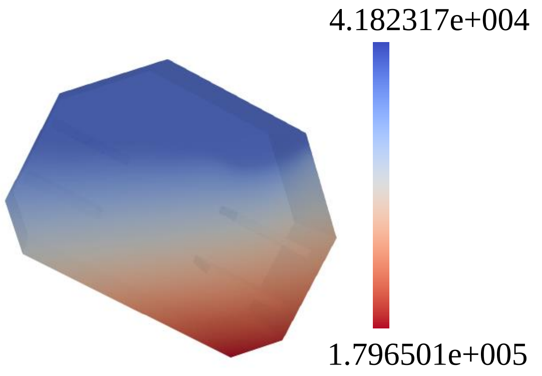

(a) Pressure at t = 5 s

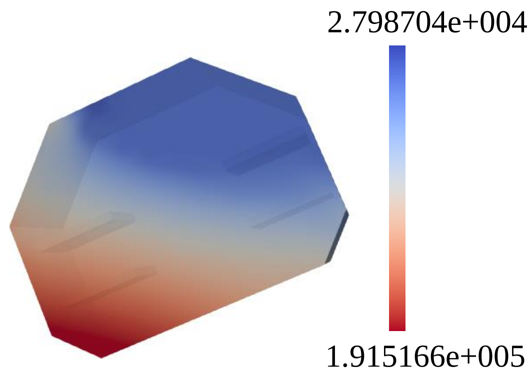

(b) Pressure at t = 10 s

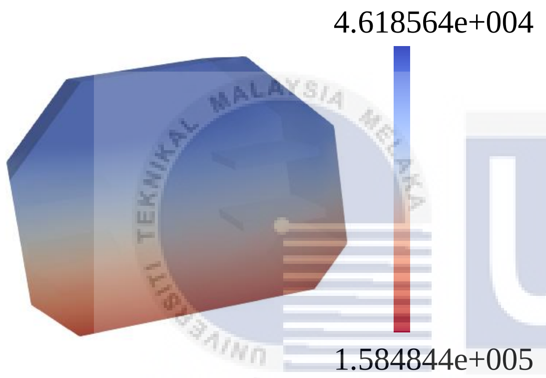

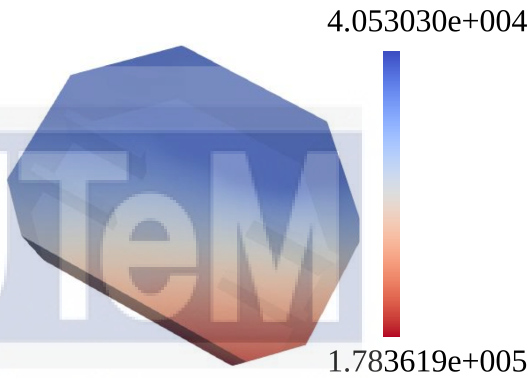

(c) Pressure at t = 15 s

(d) Pressure at t = 20 s

Figure 4.30 Pressure at t = 5 s until t = 20 s for horizontal baffles in 75% filling level of LNG in Pa

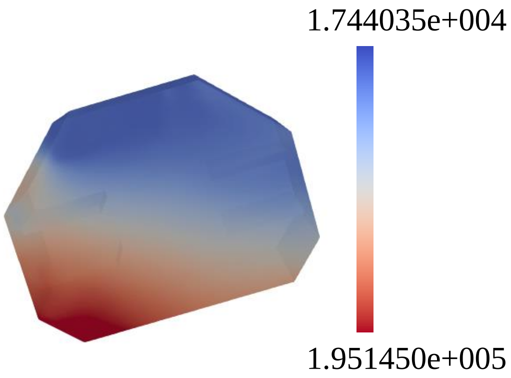

(e) Pressure at t = 25 s

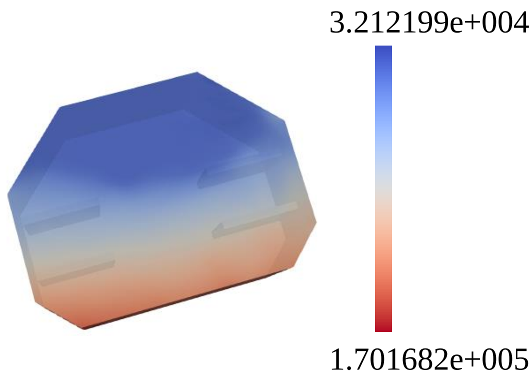

(f) Pressure at t = 30 s

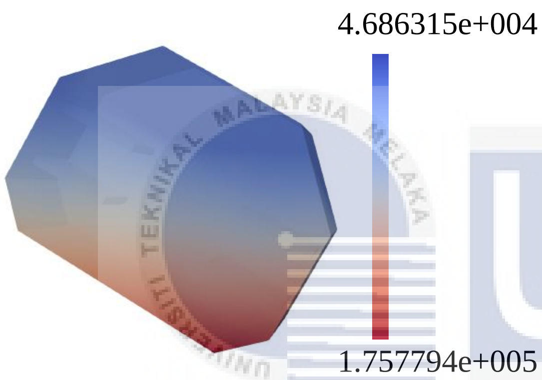

(g) Pressure at t = 35 s

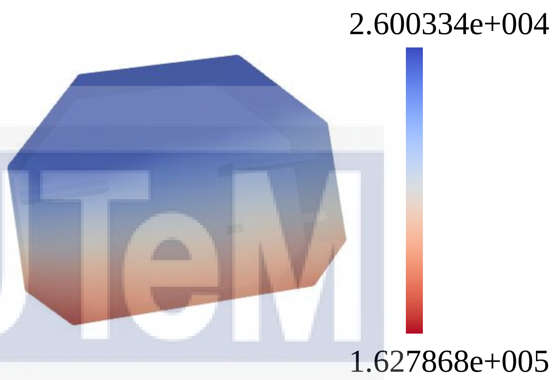

(h) Pressure at t = 40 s

Figure 4.31 Pressure at t = 25 s until t = 40 s for horizontal baffles in 75% filling level of LNG in Pa

4.4.2 Vertical baffles

When simulating the tank with vertical baffles, the result shows that the tank experienced highest pressure at t = 25 s with 2.71 x 10^5 Pa as in Figure 4.32. The sloshing phenomenon start with a stable pressure until t = 20 s, but at t = 25 s, the pressure increase until 2.71 x 10^5 Pa and then reduces to 1.75 x 10^5 Pa and become stable until t = 40 s. The sloshing diagrams are shown in Figure 4.33 until Figure 4.36.

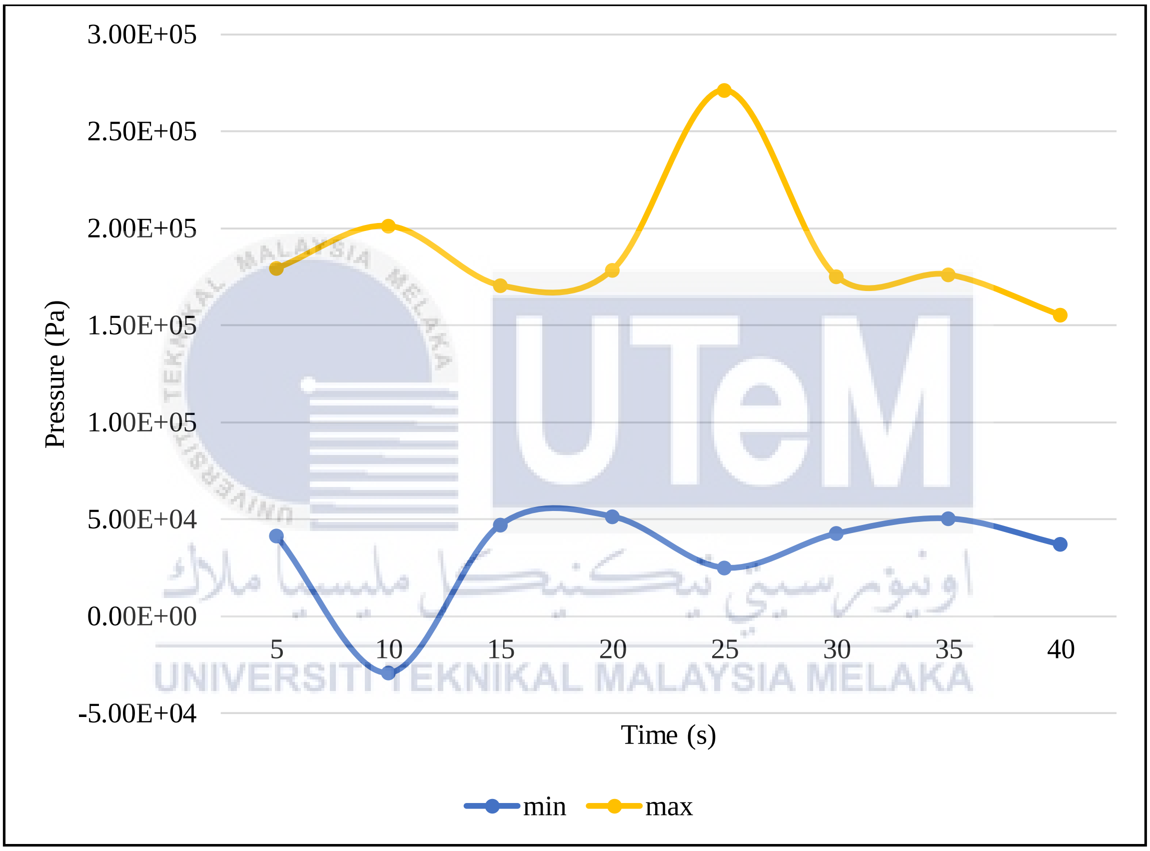

Figure 4.32 Pressure of LNG with vertical baffles against time

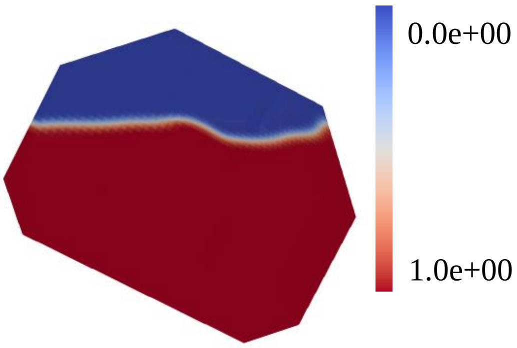

(a) Phase fraction at t = 5 s

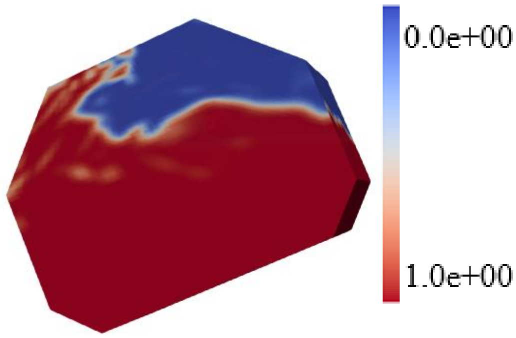

(b) Phase fraction at t = 10 s

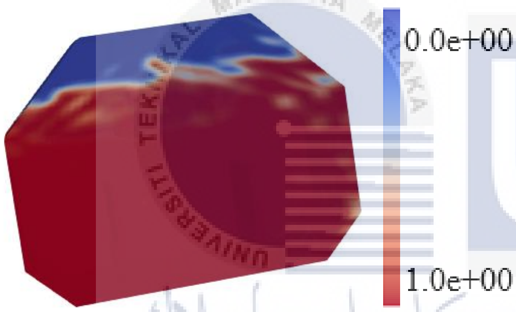

(c) Phase fraction at t = 15 s

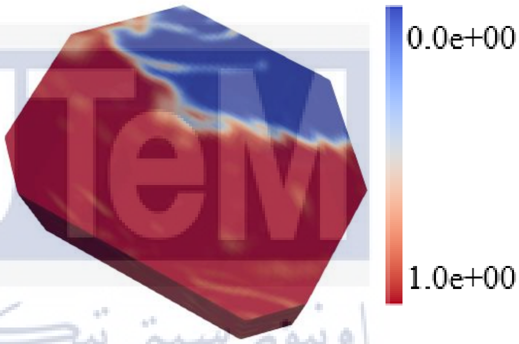

(d) Phase fraction at t = 20 s

Figure 4.33 Phase fraction at t = 5 s until t = 20 s

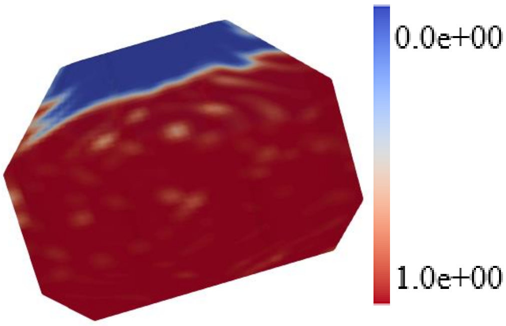

(e) Phase fraction at t = 25 s

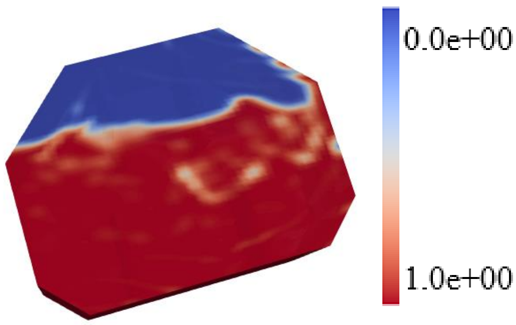

(f) Phase fraction at t = 30 s

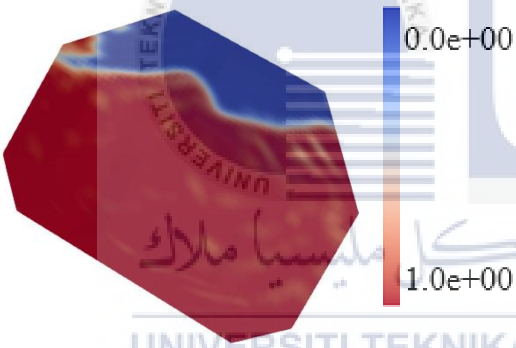

(g) Phase fraction at t = 35 s

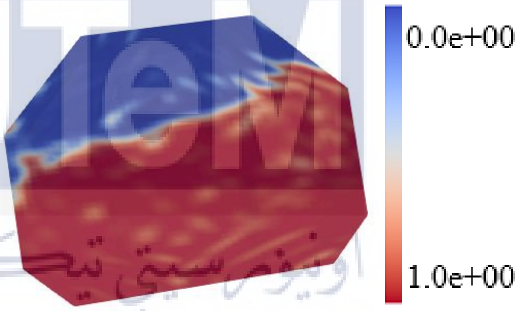

(h) Phase fraction at t = 40 s

Figure 4.34 Phase fraction at t = 25 s until t = 40 s

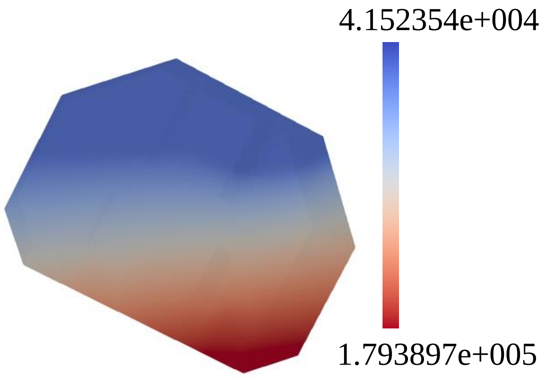

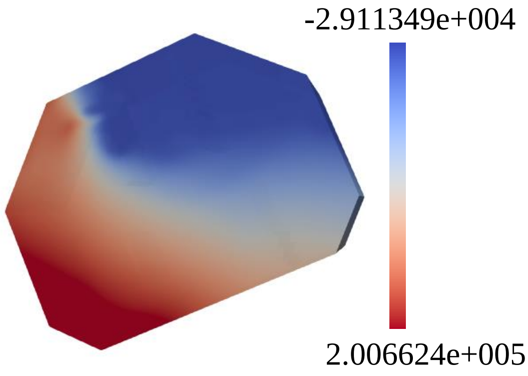

(a) Pressure at t = 5 s (b) Pressure at t = 10 s

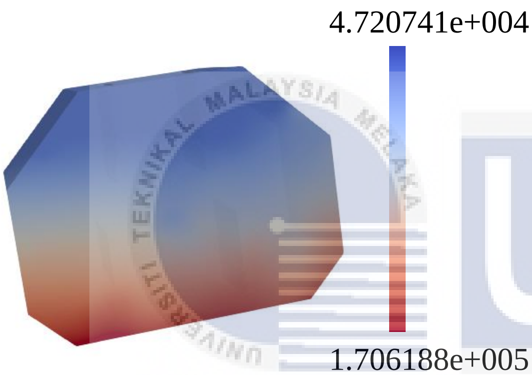

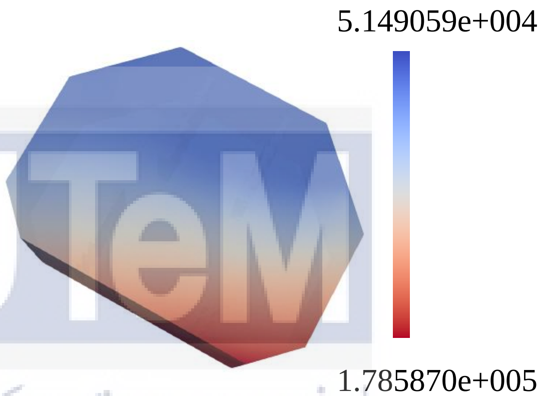

(c) Pressure at t = 15 s (d) Pressure at t = 20 s

Figure 4.35 Pressure at t = 5 s until t = 20 s for vertical baffles in 75% filling level of LNG in Pa

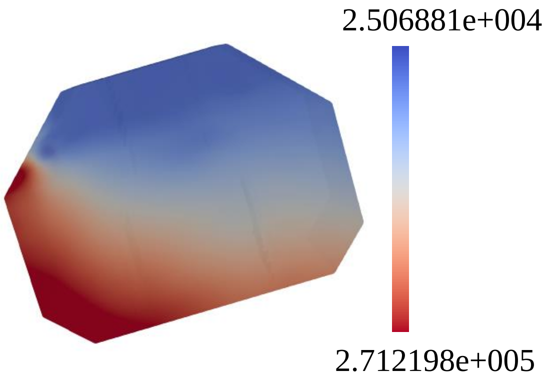

(e) Pressure at t = 25 s

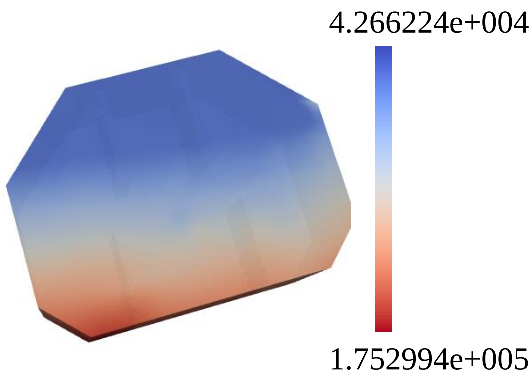

(f) Pressure at t = 30 s

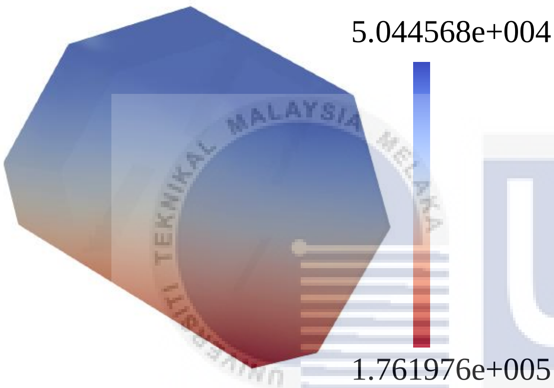

(g) Pressure at t = 35 s

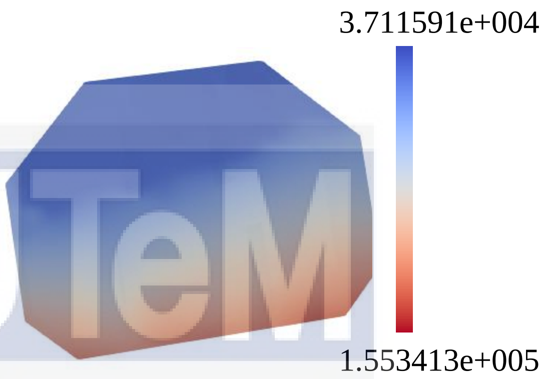

(h) Pressure at t = 40 s

Figure 4.36 Pressure at t = 25 s until t = 40 s vertical baffles in 75% filling level of LNG in Pa

4.4.3 Combinatorial baffles

The result shows that the pressure of the tank with combinatorial baffles is quite stable from the start as in Figure 4.37. Minimum pressure also in slightly stable condition. But, minimum and maximum pressure on this condition have a big difference. The highest maximum pressure occurred when t = 10 s with 1.88×10^5 Pa then followed with 1.83×10^5 Pa at t = 20 s. Thus, the condition is stable compare to the other types of baffles. The phase fraction and pressure diagram shown in Figure 4.38 until Figure 4.41.

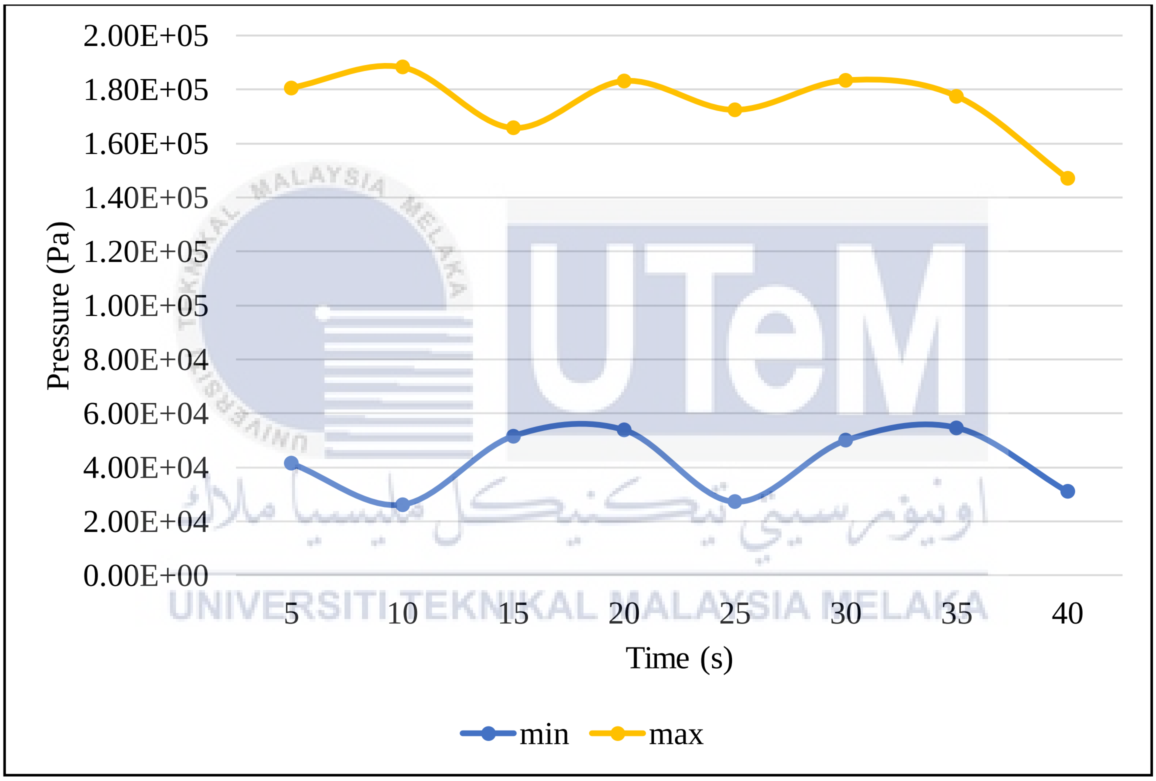

Figure 4.37 Pressure of LNG with combinatorial baffles against time

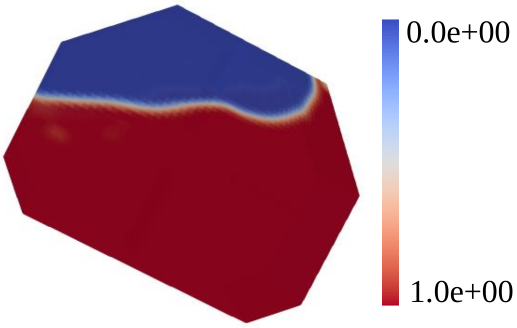

(a) Phase fraction at t = 5 s

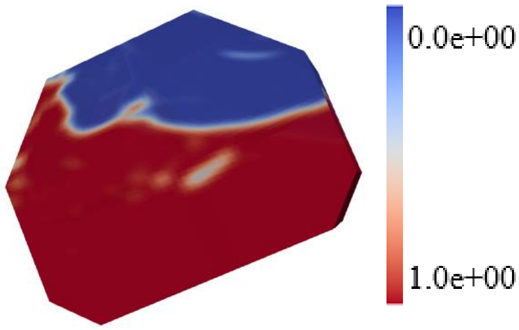

(b) Phase fraction at t = 10 s

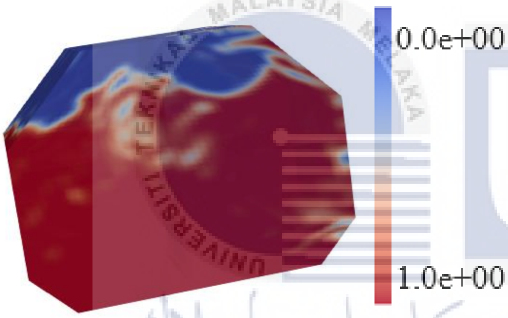

(c) Phase fraction at t = 15 s

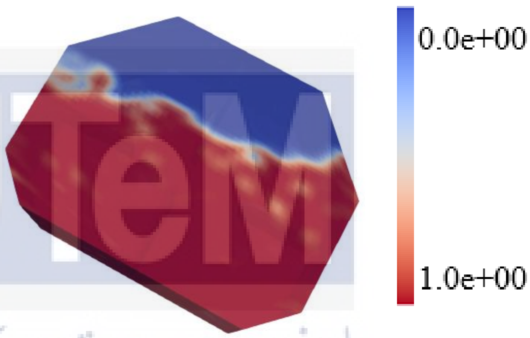

(d) Phase fraction at t = 20 s

Figure 4.38 Phase fraction at t = 5 s until t = 20 s

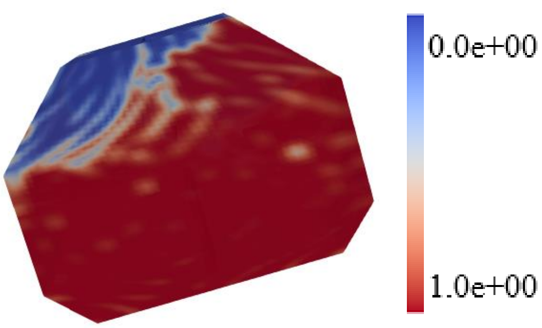

(e) Phase fraction at t = 25 s

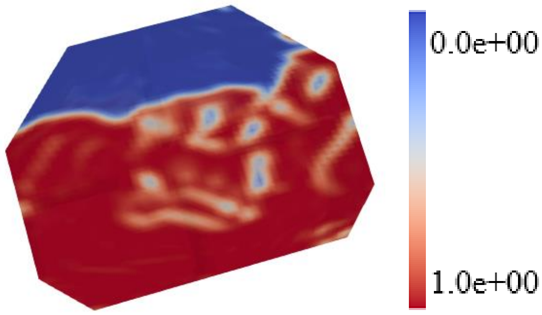

(f) Phase fraction at t = 30 s

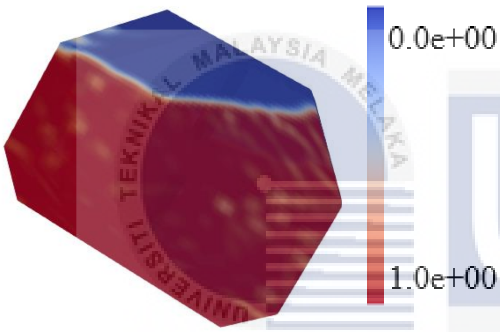

(g) Phase fraction at t = 35 s

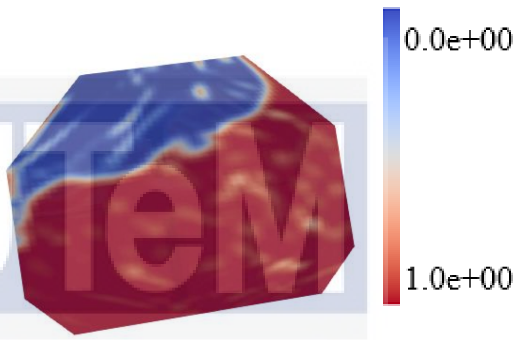

(h) Phase fraction at t = 40 s

Figure 4.39 Phase fraction at t = 25 s until t = 40 s

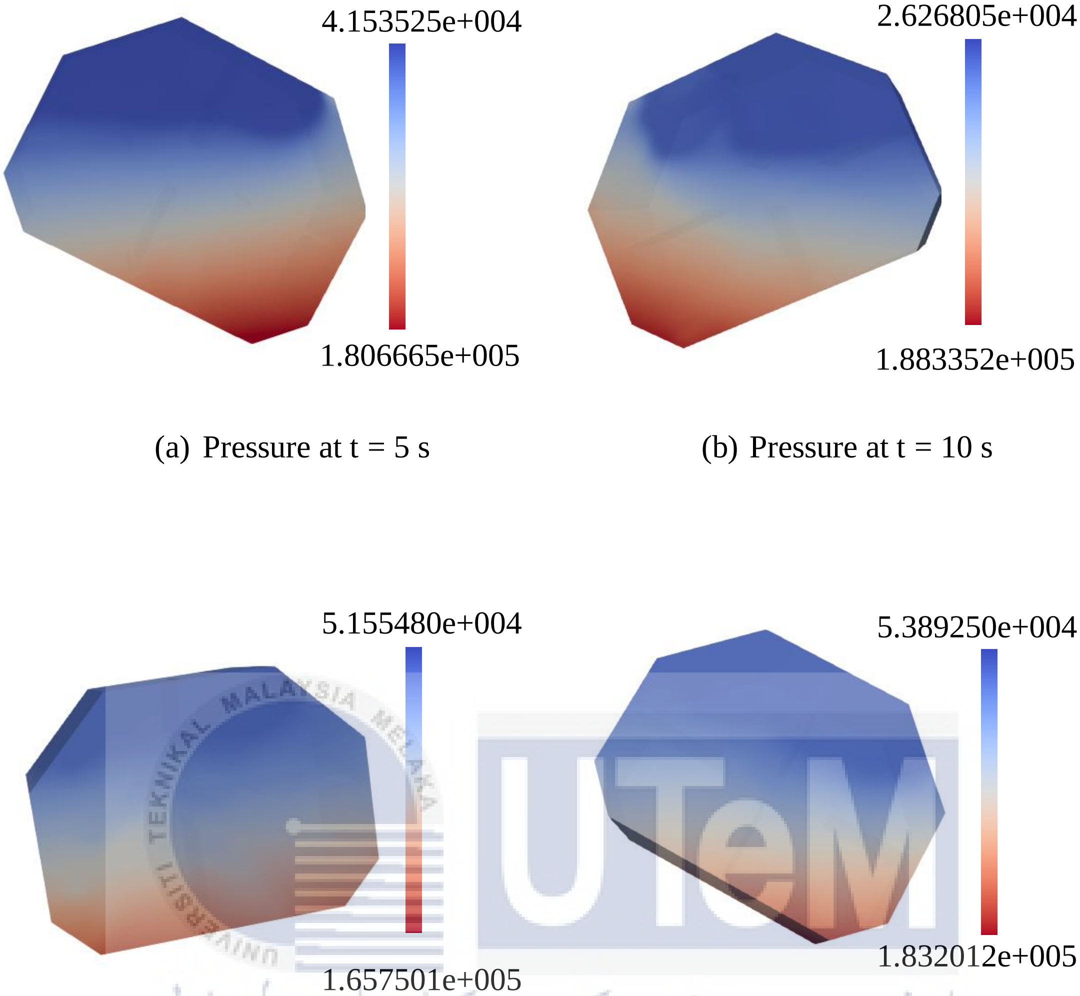

(a) Pressure at t = 5 s

(b) Pressure at t = 10 s

(c) Pressure at t = 15 s

(d) Pressure at t = 20 s

Figure 4.40 Pressure at t = 5 s until t = 20 s for combinatorial baffles in 75% filling level of LNG in Pa

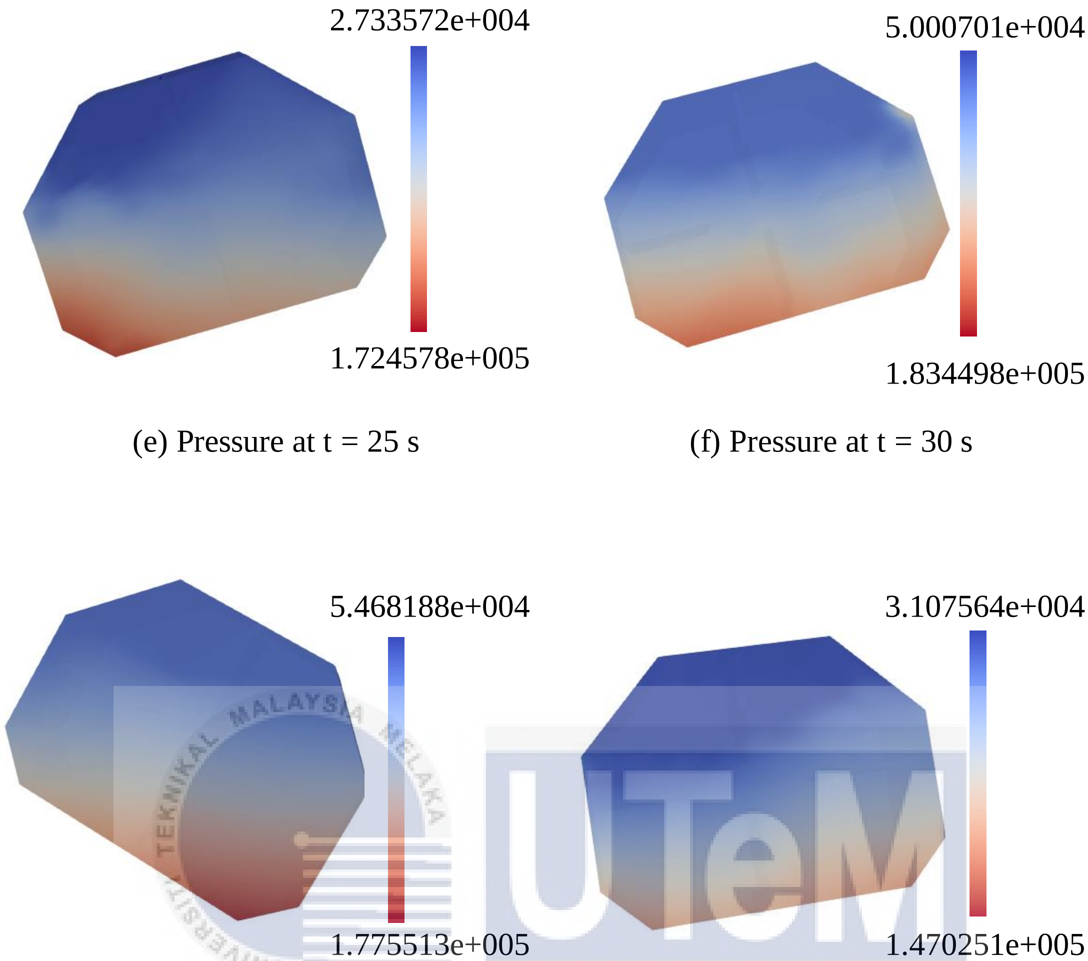

(e) Pressure at t = 25 s

(f) Pressure at t = 30 s

(g) Pressure at t = 35 s

(h) Pressure at t = 40 s

Figure 4.41 Pressure at t = 25 s until t = 40 s for combinatorial baffles in 75% filling level of LNG in Pa

4.5 Comparison between all types of baffles

From the Figure 4.42 below, the result shows that the tank with no baffles is in unstable condition because the pattern of the pressure is not maintain. In this case, the wall of the tank has high tend to break or crack. Also from the result of vertical baffles, the pressure from the start at t = 5 s until t = 20 s are quite stable, but the pressure suddenly increase when t = 25 s. Then, the pressure become stable. At this point which is at t = 25 s, the pressure is very high and possibly can lead the wall of the tank to crack. From the figure below, we can see that the pattern of pressure of horizontal baffles is somewhat stable but the pressure difference between each second is not steady. While, the combinatorial baffles, the pressure difference of each second is not much difference compare to the horizontal baffles.

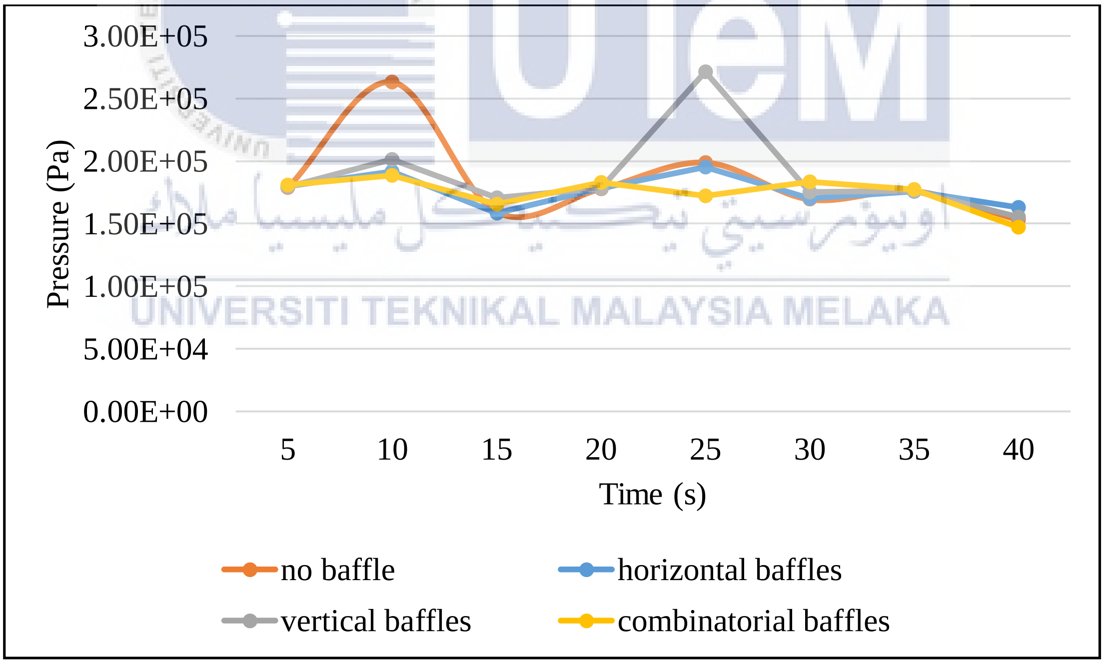

Figure 4.42 Pressure difference between baffles' types against time

CHAPTER 5

CONCLUSION AND RECOMMENDATION

5.1 Conclusion

The physical exact principles involved in creating high and low sloshing pressures are significantly different. High pressure is associated with flows all along tank boundaries toward the sharp discontinuity in the tank geometry. The drastic change throughout the direction of the fluid momentum when the discontinuity passes helps generate the signals of high pressure. The low pressures measured in this study are related directly to overhanging structures and structures that obstruct the inflow from the immediate surroundings following fluids accelerated by gravity downwards. This study starting with simulation of pressure of the LNG tank with various filling level which are 25%, 50%, 75% and 90%. The simulation gives the result that between these filling level, 75% filling level of LNG obtained the highest maximum pressure with 2.63 x 10^5 Pa at t = 10 s compared to the others filling level. Furthermore, in this study, a two-phase fluid flow code then used to simulate 3D liquid sloshing phenomena with complicated baffles such as perforated vertical baffle, horizontal baffle and combinatorial baffle. The most extreme impact pressure is observed to occur at the lower left and lower right chamfer. In addition, the maximum pressure of impact acting on occurred at the tank wall for the case of without baffle and in the case of vertical baffles. Comparing the results of various types of baffles to the no baffle case, the pressure of the use of vertical baffles decrease by 23% while horizontal baffles and combinatorial baffles greatly reduced by 26% and 28% respectively. From the results obtained, combinatorial baffles is the type of baffles that can reduced the pressure of LNG tank.

5.2 Recommendation

For future works, the existence of baffles should be used in a LNG tank to improve the pressure during the sloshing phenomenon. Furthermore, the designing of the baffles need to be accurate and corresponding to the tank in order to reduce the pressure and to avoid the unwanted incident such as the cracking or breaking of tank's wall.

REFERENCES

Kim, J. W., Shin, Y. S., & Bai, K. J. (2002, January 1). A Finite-Element Computation For the Sloshing Motion In LNG Tank. International Society of Offshore and Polar Engineers.

Tanaka, T. et al 1988 Estimation of Impact Pressure and Hydrodynamic Force due to Sloshing in LNG Carrier, Nippon Kokan Technical Report, *Overseas* No. 42.

Peric, M., Zorn, T., el Moctar, O., Schellin, T. E., and Kim, Y. (May 28, 2009). "Simulation of Sloshing in LNG-Tanks." ASME. *J. Offshore Mech. Arct. Eng*. August 2009; 131(3): 031101.

Mikelis, N. E. 1984 Sloshing in partially filled liquid tanks and its effect on ship motions: Numerical simulations and experimental verification. RINA Spring meeting, London

Faltinsen, O. M. and Rognebakke O. F. 2000 *Sloshing*, Int. Conf. on Ship and Shipping Research - NAV, Venice, Italy.

Hinatsu, M., Tsukada, Y., Fukasava, R., and Tanaka, Y., 2001, “Experiments of Two Phase Flows for the Joint Research,” *Proceedings of the SRI-TUHH Mini-Workshop on Numerical Simulation of Two-Phase Flows*, Ship Research Institute, Tokyo.

LI, Yu-long, Ren-chuan ZHU, Guo-ping MIAO, and Ju FAN. "Simulation of tank sloshing based on OpenFOAM and coupling with ship motions in time domain", Journal of Hydrodynamics Ser B, 2012.

Mi-an Xue, Peng-zhi Lin, Jin-hai Zheng, Yuxiang Ma, Xiao-li Yuan, Viet-Thanh Nguyen. "Effects of perforated baffle on reducing sloshing in rectangular tank: Experimental and numerical study", China Ocean Engineering, 2013

Ge Liu, Yan Lin, Guan Guan and Yan-yun Yu Journal: Journal of Zhejiang University SCIENCE A, 2018, Volume 19, Number 10, Page 758

Kim, Y., 2001. Numerical simulation of sloshing flows with impact load, *Appl. Ocean Res.*, **23**(1): 53–62.

Kim, H. S. and Lee, Y. S., 2008. Optimization design technique for reduction of sloshing by evolutionary methods, *J. Mech. Sci. Tech.*, **22**(1): 25–33.

N.E. Mikelis, J.K. Miller, K.V. Taylor., *Sloshing in partially filled liquid anks and its effect on ship motions: numerical simulation andexperimental verification*, Royal Institution of Naval ArchitectsTransactions, 126, pp. 267-277, 1984.

E.W. Graham and A.M. Rodriguez., *The characteristics of fuel motion which affect airplane dynamics*, Journal of applied mechanics, Sep, pp.381-388, 1952

M.Y. Tan, Y.P. Xiong, J.T. Xing., *Dynamic response analysis of an onshore LNG-storage tank interaction system subject to impact or earthquake loads*, 16th International Congress on Sound and Vibration, Krakow, Poland, 2009.

Wang, W., & Xiong, Y. P. (2014). Minimising the sloshing impact in membrane LNG tank using a baffle.

Sohn, J. M., Bae, D. M., Bae, S. Y., & Paik, J. K. (2017). Nonlinear structural behaviour of membrane-type LNG carrier cargo containment systems under impact pressure loads at− 163 C. *Ships and Offshore Structures*, *12*(5), 722-733.

Khan, M. S., Effendy, S., Karimi, I. A., & Waz waz, A. (2019). Improving design and operation at LNG regasification terminals through a corrected storage tank model. *Applied Thermal Engineering*, *149*, 344-353.

Hu, Z. Q., Wang, S. Y., Chen, G., Chai, S. H., & Jin, Y. T. (2017). The effects of LNG-tank sloshing on the global motions of FLNG system. *International Journal of Naval Architecture and Ocean Engineering*, *9*(1), 114-125.

Lee, J. H., Choi, J. H., Han, S. K., Choi, D. K., & Moon, Y. S. (2019). *U.S. Patent No. 10,352,499*. Washington, DC: U.S. Patent and Trademark Office.

Arai, M., Cheng, L. Y., Wang, X., Okamoto, N., Hata, R., & Karuka, G. (2016). Sloshing and swirling behavior of liquid in a spherical LNG tank. *Proceedings of PRADS2016*, *4*, 8th.

Lv, D., Tan, W., Liu, L., Zhu, G., & Peng, L. (2017). Research on maximum explosion over pressure in LNG storage tank areas. *Journal of Loss Prevention in the Process Industries*, *49*, 162-170.

Liu, G., Lin, Y., Guan, G., & Yu, Y. Y. (2018). Numerical research on the anti-sloshing effect of a ring baffle in an independent type C LNG tank. *Journal of Zhejiang University-SCIENCE A*, *19*(10), 758-773.

Karlsson, S., Jansson, M., Råholm, M., & Ingvar, Ö. S. T. (2017). *U.S. Patent No. 9,702,506*. Washington, DC: U.S. Patent and Trademark Office.

Kim, J., Kim, Y., Kim, S. Y., Lee, K. M., & Sung, Y. J. (2020). Experimental Study of Slosh-induced Loads on an LNG Fuel Tank of a Container Ship. *International Journal of Offshore and Polar Engineering*, *30*(02), 141-148.

Zhuang, Y., & Wan, D. (2019). Numerical study on ship motion fully coupled with LNG tank sloshing in CFD method. *International Journal of Computational Methods*, *16*(06), 1840022.

Zalar, M., CAMBOS, P., BESSE, P., LE GALLO, B., & MRAVAK, Z. (2005, March). Partial Fillings of Membrane Type LNG Carriers. In *21st GASTECH Conference, Bilbao, Spain*.

LIST OF APPENDICES

APPENDIX A
PROGRAM FOR THE TANK

```
#!/bin/sh
cd ${0%/*} || exit 1    # Run from this directory

# Source tutorial run functions
. $WM_PROJECT_DIR/bin/tools/RunFunctions

m4 system/blockMeshDict.m4 > system/blockMeshDict
runApplication blockMesh
cp 0/alpha.water.orig 0/alpha.water
runApplication setFields
runApplication `getApplication`
```

APPENDIX C

PROGRAM FOR BLOCKMESH

```
// * * * * * * * * * * * * * * * * * * * * * * * * * * * * * *
* * * * * * * * //
Create time

Creating block mesh from
    "C:/PROGRA~1/BLUECF~1/ofuser-of5/run/sloshingTank3D6DoF-
25/system/blockMeshDict"
No non-linear block edges defined
No non-planar block faces defined
Creating topology blocks
Creating topology patches

Reading patches section

Creating block mesh topology

Reading physicalType from existing boundary file

Default patch type set to empty

Check topology

     Basic statistics
          Number of internal faces : 2
          Number of boundary faces : 14
          Number of defined boundary faces : 14
          Number of undefined boundary faces : 0
     Checking patch -> block consistency

Creating block offsets
Creating merge list .

Creating polyMesh from blockMesh
Creating patches
Creating cells
Creating points with scale 1
    Block 0 cell size :
        i : 0.6 .. 0.6
        j : 0.441942 .. 0.441942
        k : 0.689655 .. 0.689655

    Block 1 cell size :
        i : 0.8 .. 0.8
        j : 0.576923 .. 0.576923
        k : 0.689655 .. 0.689655
```

```
    Block 2 cell size :
        i : 0.8 .. 0.8
        j : 0.642824 .. 0.642824
        k : 0.689655 .. 0.689655


There are no merge patch pairs edges

Writing polyMesh
----------------
Mesh Information
----------------
  boundingBox: (-10 -20 -10) (10 20 20)
  nPoints: 99450
  nCells: 92800
  nFaces: 284906
  nInternalFaces: 271894
----------------
Patches
----------------
  patch 0 (start: 271894 size: 13012) name: walls

End
```

APPENDIX C

PROGRAM FOR SETING UP THE FILLING LEVEL

```
// * * * * * * * * * * * * * * * * * * * * * * * * * * * * * * *
* * * * * * * * //
Create time

Create mesh for time = 0

Reading setFieldsDict

Setting field default values
    Setting internal values of volScalarField alpha.water

Setting field region values
    Adding cells with center within boxes 1((-100 -100 -100)
(100 100 0))
    Setting internal values of volScalarField alpha.water

End
```